European Journal of Medicinal Chemistry 127 (2017) 100–114

Contents lists available at ScienceDirect

European Journal of Medicinal Chemistry

journal homepage: http://www.elsevier.com/locate/ejmech

Research paper

Synthesis and biological evaluation of curcumin inspired indole analogues as tubulin polymerization inhibitors

P.V. Sri Ramya [a], Srinivas Angapelly [a], Lalita Guntuku [b], Chander Singh Digwal [a], Bathini Nagendra Babu [a], V.G.M. Naidu [b, **], Ahmed Kamal [a, *]

[a] Department of Medicinal Chemistry, National Institute of Pharmaceutical Education and Research (NIPER), Hyderabad 500037, India
[b] Department of Pharmacology and Toxicology, National Institute of Pharmaceutical Education and Research (NIPER), Hyderabad 500037, India

ARTICLE INFO

Article history:
Received 19 November 2016
Received in revised form
19 December 2016
Accepted 21 December 2016
Available online 23 December 2016

Keywords:
Curcumin mimics
Indole
Cytotoxic
Apoptosis
Cell cycle
Claisen-Schmidt condensation

ABSTRACT

In our endeavour towards the development of potent cytotoxic agents, a series of some new curcumin inspired indole analogues, in which indole and phenyl moieties are linked on either sides of 1,5-diaryl-1,4-pentadien-3-one system have been synthesized and characterized by spectral data. All the newly synthesized analogues were tested for their cytotoxic potential against a panel of eight cancer cell lines namely, lung (A549), breast (MDA-MB-231, BT549 and 4T1), prostate (PC-3, DU145), gastric (HGC-27) and cervical (HeLa). Notably, among all the compounds tested, compounds **11c**, **11d** and **11f** showed potent growth inhibition on PC-3 and BT549 with IC_{50} values in the range of 3.12–6.34 μM and 4.69–8.72 μM respectively. The most active compound (**11c**) was also tested on RWPE-1 (normal prostate) cells and was found to be safe compared to the PC-3 cells. In tubulin polymerization assay, compounds **11c** and **11f** effectively inhibited microtubule assembly with IC_{50} values of 10.21 ± 0.10 and 8.83 ± 0.06 μM respectively. The results from molecular modelling studies revealed that these compounds bind at the colchicine binding site of the tubulin. Moreover, DAPI and acridine orange/ethidium bromide staining studies indicated that compounds **11c** and **11f** can induce apoptosis in PC-3 cells. Further flow-cytometry analysis revealed that compound **11c** arrests PC-3 cells in G2/M phase of the cell cycle while compound **11f** treatment resulted in moderate increase in the G2/M population. Additionally, the treatment by these compounds led to the impairment of mitochondrial membrane potential (DΨm) in PC-3 cells.

1. Introduction

Curcumin (**1**, Fig. 1), the active ingredient in the traditional herbal remedy and dietary Indian spice turmeric, is originally isolated from the rhizomes of *Curcuma longa* [1]. Curcumin, the principal curcuminoid of turmeric and its derivatives are characterized by a wide range of medicinal properties such as antimicrobial [2,3], anticancer [4], antioxidant [5], anti-inflammatory [6,7] and anti-HIV [8] activities. Moreover, curcumin has been reported to influence many cell-signaling pathways such as NF-kB, STAT, TNF-α and regulates the expression of p53 tumor suppressing gene [9,10]. Also, curcumin exhibits therapeutic promise for prostate cancer by interfering with cell proliferation, development of metastasis through the down-regulation of androgen receptor and epidermal growth factor receptor, but also through the induction of cell cycle arrest [11,12]. Although, curcumin is a potent anticancer agent with remarkable safety profile, it is highly metabolically unstable and has poor systemic bioavailability that prevents itself from becoming a clinical chemotherapeutic [13]. This has triggered extensive research in search for curcumin analogues/mimics with improved potency and pharmacokinetic profiles for the potential clinical treatment of cancers [14–25].

Attempts have been made by researchers to chemically modify curcumin in order to improve its activity against cancer. In this process, a number of curcumin analogues have been synthesized and studied for their chemopreventive effects [14–16]. Curcumin mimic **3** (Fig. 1) differs from curcumin in having a five-carbon dienone linear linker instead of a seven-carbon β-diketone linker, showed 5–5.5 fold increase in the cytotoxic potency relative to curcumin towards PC-3 cell line [17]. Further, curcumin analogues

* Corresponding author.
** Corresponding author.
E-mail address: ahmedkamal@iict.res.in (A. Kamal).

http://dx.doi.org/10.1016/j.ejmech.2016.12.043
0223-5234/

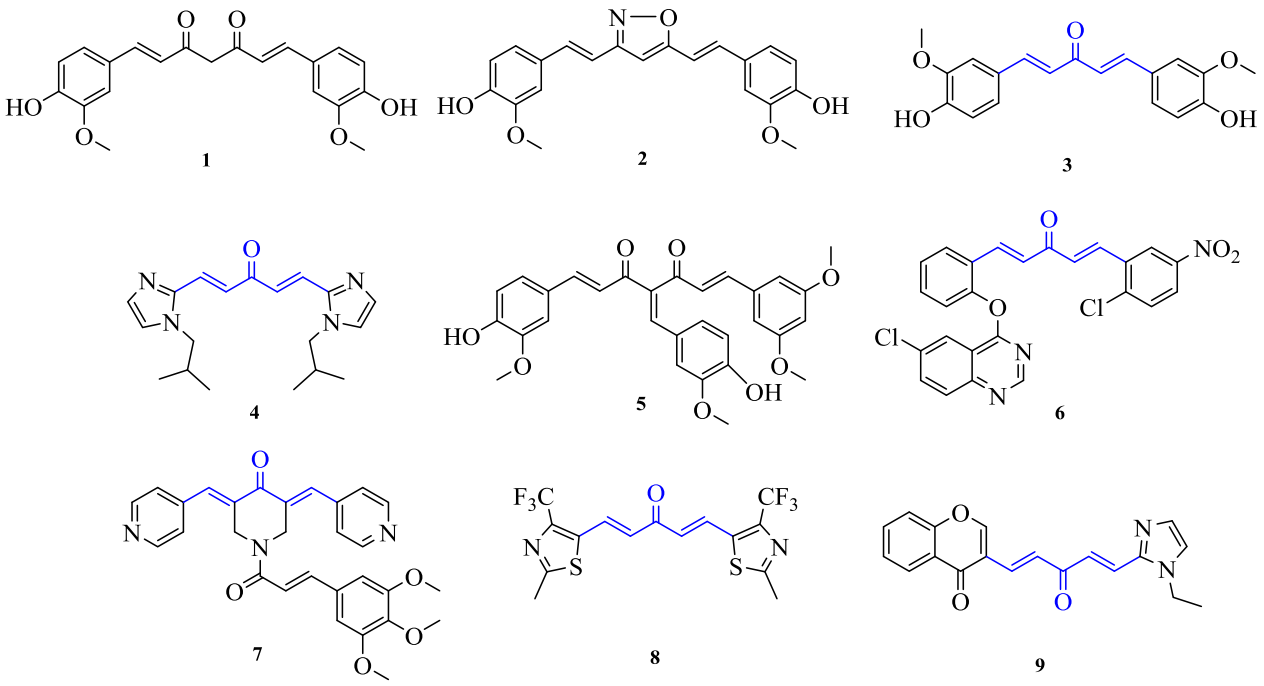

Fig. 1. Structure of curcumin and its analogues/mimics.

possessing imidazole [18], quinazoline [19], resveratrol [20], piperidone [21], thiazole [22] and chromone [23] moieties have been well documented in the literature for their enhanced potency than curcumin. From these observations, it can be noticed that 1,5-diheteroaryl/arylheteroaryl penta-1,4-dien-3-one, represented by these compounds (Fig. 1, curcumin analogues **3**–**4** and **6**–**9**), is an optimal scaffold for developing curcumin mimics as potential antitumor agents due to their superior *in vitro* potency and better pharmacokinetic profiles compared to curcumin. It is therefore very meaningful to launch in-depth investigation of this class of curcumin mimics as potential drug candidates for the treatment of cancer.

On the other hand, the chemistry of indole/its derivtaives has received substantial attention due to their synthetic and effective biological importance. Compounds bearing this ring display a variety of biological activities such as anti-inflammatory [24], antimicrobial [25], anticancer [26], antiHIV [27], antioxidant [28] and antitubercular [29]. Therapeutically interesting drug candidates; for example (Fig. 2), vincristine [30], vinblastine [31], panobinostat [32] (anti-tumor), vincamine (antihypertensive) [33], pindolol (antidepressant) [34], ateviridine (antiHIV) [35] and siramesine (antidepressant) [36] are known to contain indole nucleus.

In this context, we desire to explore the pharmacophoric potential of curcumin inspired indole analogues (Fig. 3) and to the best of our knowledge, these analogues have not been described in the literature yet. Herein, we report the synthesis of a series of novel curcumin inspired indole analogues, possessing a five-carbon dienone linear linker attached to indole/indole derivative and phenyl ring on either sides of it to give 1,5-arylheteroarylpenta-1,4-dien-3-ones and evaluated for their cytotoxic activity on selected human cancer cell lines.

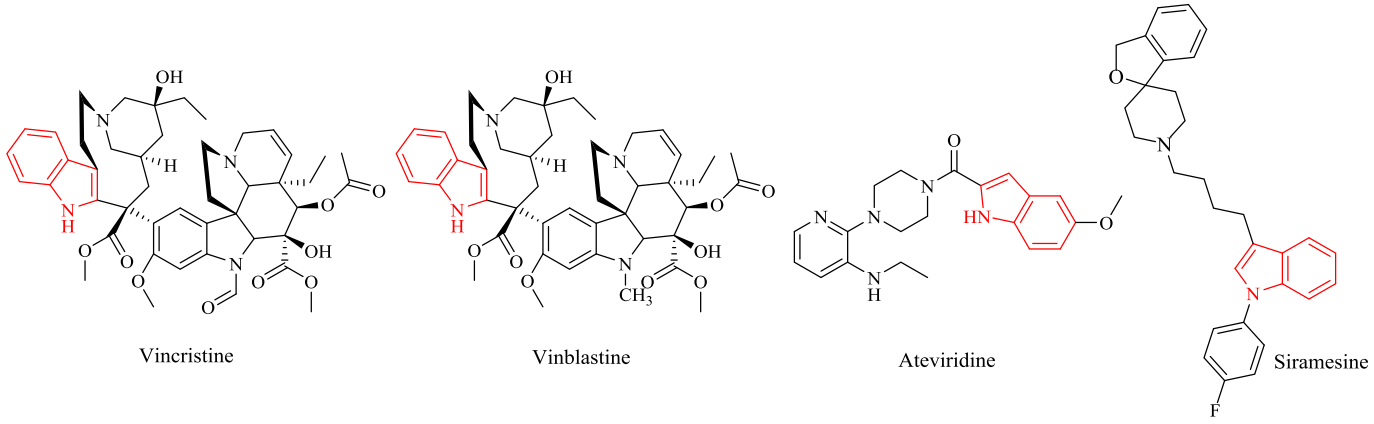

Fig. 2. Structure of some representative bioactive compounds possessing indole moiety.

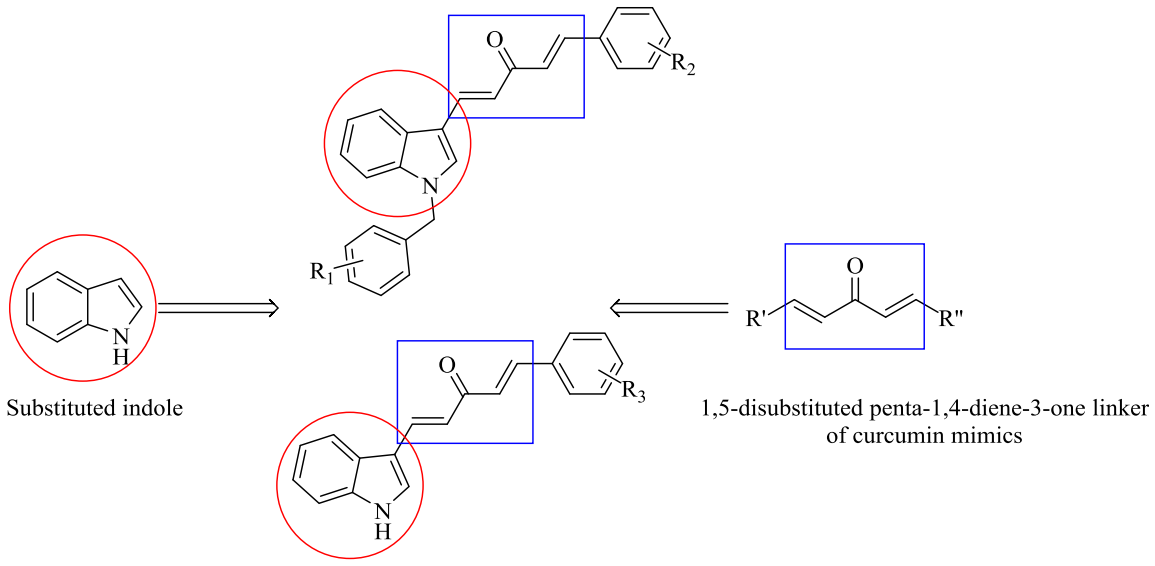

Fig. 3. Design of novel curcumin inspired indole analogues as anticancer agents.

2. Results and discussion

2.1. Chemistry

Two core structural elements (i) an aldehyde, and (ii) a substituted chalcone are required for achieving the target compounds (1*E*,4*E*)-1-(1-benzyl-1*H*-indol-3-yl)-5-phenylpenta-1,4-dien-3-one (**9a-s**) and (1*E*,4*E*)-1-(1*H*-indol-3-yl)-5-phenylpenta-1,4-dien-3-one (**11a-f**). Initially, for the preparation of aldehydes (**5**), the appropriately substituted benzaldehydes (**1**) were reduced [37] to produce corresponding alcohols (**2**), which were then treated with phosphorous tribromide [38] to furnish the benzyl bromide derivatives (**3**). Then N-benzylation of 1H-indole-3-carboxaldehyde (**4**) with benzyl bromides (**3**) in the presence of NaH [39] produced the target aldehydes (**5**). Chalcones **8a-f** were prepared by NaOH-catalysed Claisen-Schmidt condensation of benzaldehyde (**6**) with acetone [40]. Similarly 1*H*-indole-3-carboxaldehyde (**4**) was treated with acetone in the presence of 15% NaOH solution to give intermediate **8g**. Finally, NaOH-catalysed Claisen-Schmidt condensation of chalcone **8** and aldehyde (**5** or **10**) furnished the target compounds **9a-s** and **11a-f** in good yields.(see Scheme 1)

All the synthesized compounds were purified by column chromatography and well characterized by spectroscopic techniques such as IR, NMR, HRMS which were in full accordance with the depicted structures. The ^{1}H NMR spectrum of (1*E*,4*E*)-1-(1-benzyl-1*H*-indol-3-yl)-5-(4-methoxyphenyl)penta-1,4-dien-3-one, **9b** showed a sharp singlet of benzylic protons at δ 5.35, a singlet of methoxy protons at δ 3.86 and rest all protons appeared in the aromatic region. In the ^{13}C NMR spectrum of **9b**, the carbonyl carbon appeared at δ 188.9 and the aromatic carbons appeared in the range of δ 141.7–110.6. Methoxy carbon and benzylic carbon appeared at δ 55.4 and 50.5 respectively. Almost similar patterns were observed in ^{1}H and ^{13}C NMR spectra of all the synthesized compounds (**9a-9s)** of this series. The ^{1}H NMR spectrum of (1*E*,4*E*)-1-(1*H*-indol-3-yl)-5-(4-methoxyphenyl)penta-1,4-dien-3-one, **11b** showed a broad singlet at δ 10.37, which is characteristic of indole N-H proton and all aromatic protons appeared in the range of 8.11–6.55. In the ^{13}C NMR spectrum of **11b**, the carbonyl carbon appeared at δ 189.0, the aromatic carbons appeared in the range of δ 141.5–112.3 and the methoxy carbon appeared at δ 55.3. Almost similar patterns were observed in ^{1}H and ^{13}C NMR spectra of rest of the compounds (**11a-11f**). A sharp band at ~1658.5 cm^{-1} in the FT-IR spectrum confirmed the presence of ketone functionality in compound **9b** whereas a broad band at 3123.5 cm^{-1} and a sharp band at ~1647 cm^{-1} confirmed the presence of N-H and ketone functionalities respectively in compound **11b**. The HRMS (ESI) of all the compounds showed an $[M+H]^{+}$ peak equivalent to their molecular formulae.

2.2. Biological evaluation

2.2.1. Evaluation of antiproliferative activity

All the synthesized compounds **9a-s** and **11a-f** were evaluated for their antiproliferative activity against a panel of tumor cell lines such as lung (A549), breast (MDA-MB-231, BT549 and 4T1), prostate (PC-3, DU145), gastric (HGC-27) and cervical (HeLa) using 3-(4,5-dimethylthiazol-2-yl)-2,5-diphenyl tetrazolium bromide (MTT) assay [41]. Concentration response course analysis was performed to determine the drug concentration required to inhibit the growth of cancer cells by 50% (IC_{50}) after incubation for 48 h. Curcumin and vincristine were used as reference standards and the assay results have been tabulated in Table 1.

In order to get the insight in to the structure-activity relationship (SAR), we varied the substitutions on both the heteroaryl and aryl rings (indole and phenyl) of these conjugates. The cytotoxic activities of compounds (**9a-s** and **11a-f)** revealed that generally *N*-benzylated indole analogues (**9a-s)** exhibited lesser activity compared to *N*-unsubstituted indole analogues (**11a-f)**. Among *N*-benzylated indole analogues (**9a-s)**, some of the synthesized compounds showed different levels of anticancer activities. Analogues without substitution (**9a-b, 9g, 9k and 9n**) or 4-chloro (**9c, 9o)** or 3-fluoro substitution on benzyl ring (**9d, 9p**) were found to be inactive towards all the tested cell lines. Also, analogues containing 4-methoxy (**9e, 9f**), 2,5-dimethoxy (**9h, 9i**), 2,4,6-trimethoxy (**9q, 9r**) substitutions on the phenyl ring were inactive on all the cell lines studied. The target compound **9j** with 4-fluoro substitution on benzyl ring and 3,4-dimethoxy substitution on phenyl ring was moderately active selectively against BT549 cell line. Further, the compound **9l** having 4-fluoro substitution on benzyl ring and 2,4,5-trimethoxy substitution on phenyl ring was found to be active on BT549, 4T1 cell lines and moderately active on

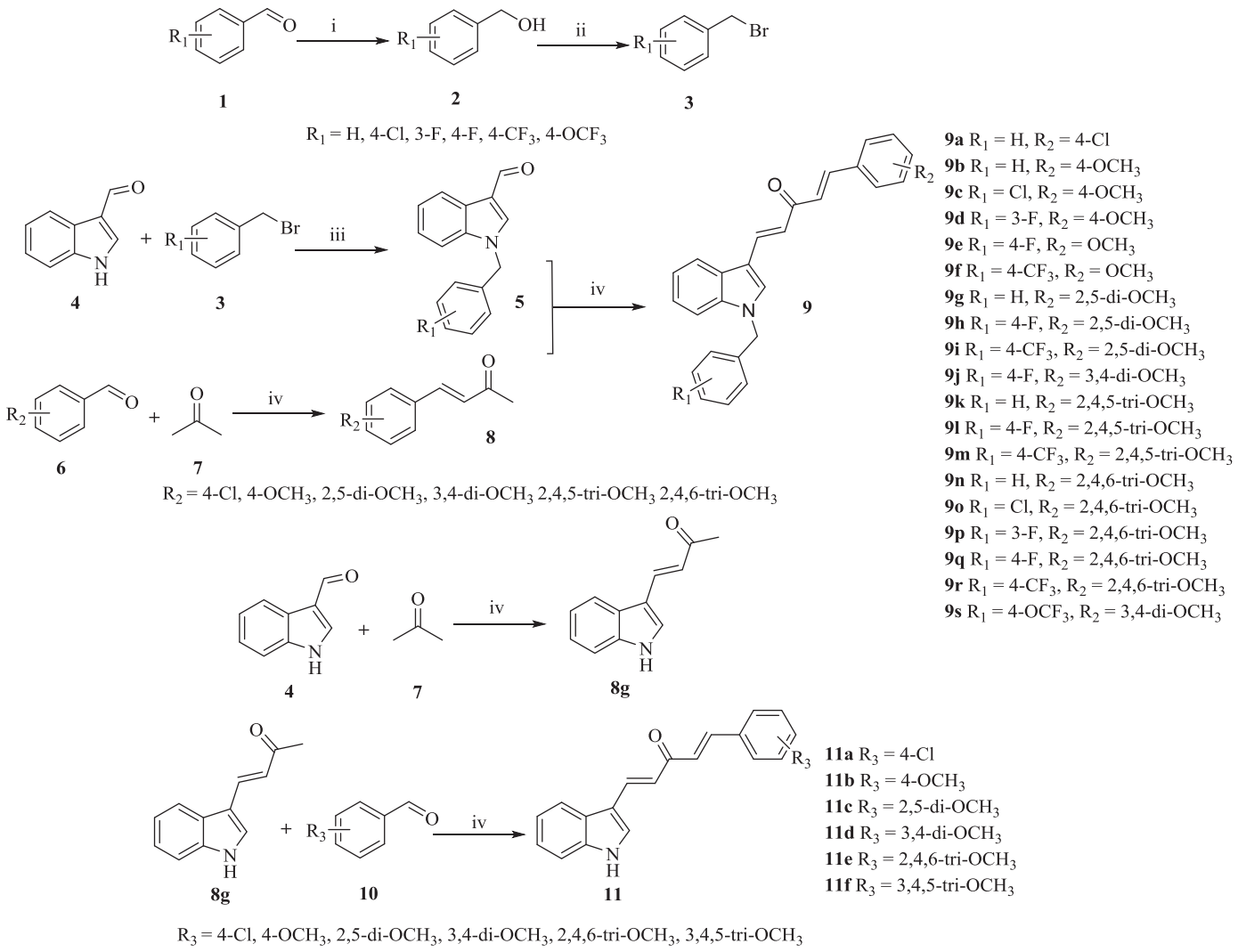

Scheme 1. Synthesis of curcumin inspired indole analogues **9a-s** and **11a-f**; Reagents and conditions: (i) $NaBH_4$, methanol, 0 °C-rt, 1 h, 94%; (ii) PBr_3, ether 0 °C-rt,1–2 h, 91%; (iii) NaH, dry DMF, 0 °C-rt, 2–3 h, 75–90%; (iv) 15% NaOH, ethanol 0 °C - rt, 2–3 h, 70–85%.

HeLa cell line. Moreover, the compound **9m** containing 4-trifluoromethyl substitution on benzyl ring and 2,4,5-trimethoxy substitution on phenyl ring was active on both BT549 and 4T1 cell lines. Additionally, the analogue **9s** with 4-trifluoromethoxy substitution on benzyl ring was found to be inactive on all the cell lines examined. Among N-unsubstituted indole (N-H) analogues (**11a-f**), analogue **11a** with 4-chloro substitution on phenyl ring was selectively active on HeLa cell line and moderately active on BT549 cell line. Analogues (**11b-f**) having electron donating substitution such as methoxy showed remarkable activity against some of the cell lines studied. Particularly, compounds **11c, 11d, 11e** and **11f** displayed potent cytotoxicity on PC-3 cell lines (IC_{50} values of 6.34, 5.52, 3.12 and 3.15 μM respectively), whereas the reference standard, curcumin displayed IC_{50} of 12.22 μM. Interestingly, compounds **11c**, **11d** and **11f** were significantly active on HGC-27 (IC_{50} of 5.21, 7.45 and 8.65 μM respectively), HeLa (IC_{50} of 6.59, 6.44 and 3.31 μM respectively) and BT549 cell lines (IC_{50} of 8.34, 4.69 and 8.72 μM respectively). The compounds (**11c** and **11f**) with promising cytotoxicity were also tested on normal prostate (RWPE-1) cells and were found to be safe compared to the PC-3 cells.

The structure-activity relationship (SAR) studies of these analogues can be summed up by stating that *N*-unsubstituted indole analogues (**11a-f)** were found to be more active than the other *N*-substituted analogues (**9a-s) (**Fig. 4**)**. The impact of substitution on phenyl ring is interesting in the light of the results of the SAR study, which demonstrates that the presence of electron donating groups such as methoxy (**11b-f)** is favourable for activity, in contrast electron withdrawing group such as 4-chloro (**11a)** resulted in significant loss of activity. Moreover, analogues [**11c** (2,5-dimethoxy), **11d** (3,4-dimethoxy), **11e** (2,4,6-trimethoxy) and **11f** (3,4,5-trimethoxy)] with increasing number of methoxy substitutions (more than one) on phenyl ring showed enhanced cytotoxicity. On the other hand, the presence of 4-methoxy (**11b**) and 2,4,6-trimethoxy substitution (**11e**) demonstrated increase in selectivity towards PC-3 cell line. Based on the promising cytotoxic activity, the most active compounds **11c-f** from this series were taken-up for further detailed studies.

Compounds **11c-f** were appraised as more potent by comparing their IC_{50} values with that of curcumin (Table 2). They are 2.4–5.3 times, 1.9 to 3.9 times, and 2.1 to 3.7 times, respectively, more potent than curcumin on human breast cancer cell line (BT549) and two human prostate cancer cell lines (PC-3 and DU145). This validates the promising scaffold containing indole and phenyl ring on each sides of a central linear dienone linker as novel curcumin

Table 1
IC_{50} values[a] (μM) of analogues 9a-s and 11a-f against selected human cancer cell lines.

Compound	A549[b]	MDA-MB-231[c]	BT549[c]	4T1[d]	PC-3[e]	DU145[e]	HGC-27[f]	HeLa[g]	RWPE-1[h]
9a	>50	>50	>50	>50	>50	>50	>50	>50	–
9b	>50	>50	40.12 ± 0.41	50.19 ± 0.46	>50	>50	>50	>50	–
9c	>50	>50	50.44 ± 0.22	>50	>50	>50	>50	50 ± 0.56	–
9d	>50	>50	40.36 ± 0.52	>50	>50	>50	>50	>50	–
9e	>50	>50	>50	>50	>50	>50	>50	>50	–
9f	>50	>50	>50	>50	>50	>50	>50	>50	–
9g	>50	>50	>50	>50	>50	>50	>50	>50	–
9h	>50	>50	50.12 ± 0.58	>50	>50	>50	>50	50.87 ± 0.64	–
9i	>50	>50	>50	>50	>50	>50	>50	>50	–
9j	>50	>50	30.12 ± 0.91	40 ± 0.87	>50	>50	50.32 ± 0.84	>50	–
9k	>50	>50	40.65 ± 0.81	40.84 ± 0.97	>50	>50	>50	50.12 ± 0.94	–
9l	50.12 ± 0.92	>50	25.12 ± 0.75	25.17 ± 0.82	>50	>50	40.19 ± 0.65	30.66 ± 0.64	–
9m	>50	>50	25.16 ± 0.84	25.92 ± 0.72	>50	>50	40.12 ± 0.92	50.56 ± 0.81	–
9n	>50	>50	>50	>50	>50	>50	>50	50.10 ± 0.35	–
9o	>50	>50	>50	>50	>50	>50	>50	40.91 ± 0.65	–
9p	>50	>50	>50	>50	>50	>50	>50	40.15 ± 0.57	–
9q	>50	>50	>50	>50	>50	>50	50.78 ± 0.47	>50	–
9r	>50	>50	>50	>50	>50	>50	>50	>50	–
9s	>50	>50	50.13 ± 0.75	>50	>50	>50	>50	50.54 ± 0.27	–
11a	>50	50.24 ± 0.76	30.12 ± 0.93	40.24 ± 0.56	>50	>50	50.01 ± 0.75	25.16 ± 0.65	–
11b	45.12 ± 2.1	32.01 ± 2.00	31.4 ± 0.29	21.55 ± 1.26	3.51 ± 0.1	13.62 ± 1.19	24.01 ± 0.45	NA	–
11c	18.96 ± 0.42	6.02 ± 0.09	8.34 ± 0.12	16.07 ± 0.21	6.34 ± 0.25	7.71 ± 0.41	5.21 ± 0.18	6.59 ± 1.03	18.61 ± 0.16
11d	30.22 ± 0.97	15.72 ± 0.46	4.69 ± 0.29	21.93 ± 0.45	5.52 ± 0.55	13.32 ± 0.18	7.45 ± 0.49	6.44 ± 0.40	–
11e	NA	46.44 ± 0.91	10.45 ± 0.31	13.94 ± 3.35	3.12 ± 0.12	NA	NA	NA	–
11f	8.01 ± 1.65	11.44 ± 0.96	8.72 ± 3.32	9.79 ± 0.5	3.15 ± 1.91	8.92 ± 0.31	8.65 ± 0.29	3.31 ± 0.04	6.42 ± 0.09
Curcumin	ND	15.81 ± 0.49	24.93 ± 0.9	ND	12.22 ± 0.11	28.41 ± 0.24	ND	25.41 ± 0.27	–
Vincristine sulphate (nM)	171.5 ± 20.1	116.6 ± 9.45	54.72 ± 1.18	ND	27.6 ± 2.4	72.3 ± 6.6	ND	ND	–

ND – Not determined.
[a] 50% inhibitory concentration after 48 h of drug treatment and mean ± SD of three individual experiments performed in triplicate.
[b] Human lung cancer cell line.
[c] Human breast cancer cell line.
[d] Mouse breast cancer cell line.
[e] Human prostate cancer cell line.
[f] Human gastric cancer cell line.
[g] Human cervical cancer cell line.
[h] Normal human prostate epithelial cells.

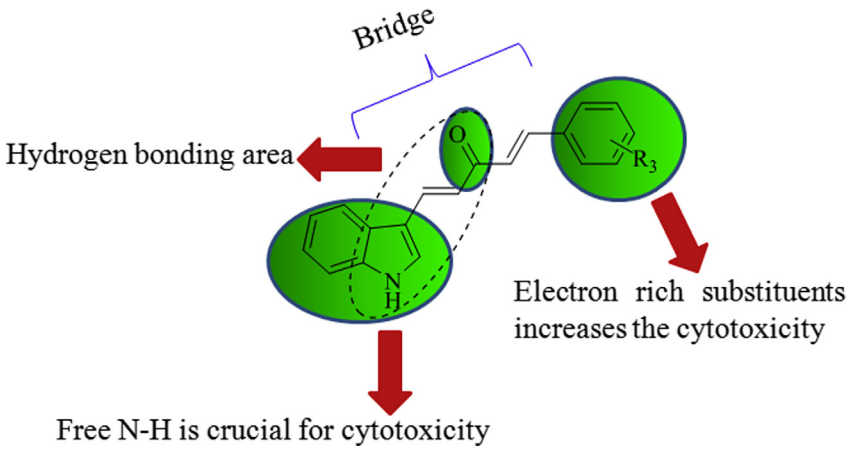

Fig. 4. SAR analysis of curcumin inspired indole analogues.

mimics with promising cytotoxic effects against cancer cells.

2.2.2. *Effect of compounds 11c, 11d and 11f on tubulin polymerization*

Tubulin is a key component of the cytoskeletal network and is important in a wide range of cellular functions including mitosis. Tubulin is the target of several small molecule anti-proliferative ligands including chalconoids, 4,5-Diaryl-3H-1,2-dithiole-3-thiones and macrocyclic bisbibenzyl analogues which have been reported recently as tubulin polymerization inhibitors [42–44]. To investigate whether the synthesized compounds are interacting with microtubule system in order to elicit antiproliferative activity, the selected compounds **11c**, **11d** and **11f** were evaluated for their tubulin polymerization inhibitory activity in a cell-free *in vitro* assay. Initially, all the compounds were screened at 10 μM and % inhibition by compounds **11c**, **11d** and **11f** at this concentration was found to be 51.7%, 39.7% and 57.3% respectively (Fig. 5).

Nocodazole and paclitaxel, were used as reference standards. The IC_{50} value was calculated from the drug concentration required for inhibiting 50% of tubulin assembly compared to control. Among

Table 2
Relative potency of curcumin mimics.

IC_{50} of curcumin/IC_{50} of compound[a]				
Compound	MDA-MB-231[c]	BT549[c]	PC-3[e]	DU145[e]
Curcumin	1	1	1	1
11c	2.6	2.9	1.9	3.7
11d	1.0	5.3	2.2	2.1
11e	0.3	2.4	3.9	NA
11f	1.4	2.8	3.9	3.2

[a] The relative potency of curcumin mimics obtained by dividing the IC_{50} value of curcumin by that of each curcumin mimic.
[c] Human breast cancer cell line.
[e] Human prostate cancer cell line.

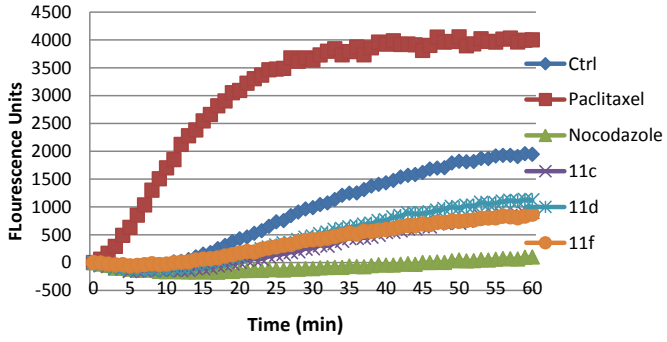

Fig. 5. % Inhibition of tubulin polymerization by compound **11c**, **11d** and **11f** at 10 μM.

Fig. 6. % Dose response inhibition of tubulin polymerization by compound **11f**.

the compounds studied, compounds **11c** and **11f** were found to be more potent inhibitors of tubulin polymerization with IC_{50} value of 10.23 ± 0.10 and 8.81 ± 0.06 μM (Fig. 6).

2.2.3. Apoptosis induction studies

Apoptosis is a process of programmed cell death that occurs in cells after suffering severe irrepairable damage to their key biomolecules and organelles. Many cytotoxic agents act by inducing the apoptosis as their common mechanism. Therefore, it was interesting to examine the apoptosis inducing effect of these compounds on PC-3 cells by the DAPI staining and acridine orange/ethidium bromide (AO/EB) staining methods.

2.2.3.1. Acridine orange and ethidium bromide staining (AO/EB). The morphological changes induced by compounds **11c** and **11f** in prostate cancer PC-3 cells were further studied by employing acridine orange/ethidium bromide (AO/EB) staining technique to deduce whether it is due to apoptosis or non-specific necrosis [45]. Acridine orange permeates through the intact cell membrane and stains the cell in green, while ethidium bromide is taken up by a cell only when the membrane integrity is impaired and tinge the nucleus red. The compound **11c** and **11f** treated as well as untreated PC-3 cells were stained with acridine orange/ethidium bromide and observed under fluorescence microscope. It can be interpreted from Fig. 7 that the control cells showed the normal healthy morphology with intact nuclear architecture and appeared green in colour whereas treated PC-3 cells have clearly demonstrated morphological changes which are the characteristic features of apoptotic cells such as condensed chromatin, cell membrane blebbing, non-uniform distribution of chromatin which marginated into a horse-shoe shaped structure and destructive fragmentation of the nuclei at 2.5 μM, 5 μM of compounds **11c** and **11f**. This confirms that both of these compounds induced cell death in PC-3 cells.

2.2.3.2. DAPI staining. To clearly examine nuclear morphological changes induced by compounds **11c** and **11f** on PC-3 cells, DAPI nuclear staining was performed. Blue-fluorescent DAPI is a nuclear stain, which can cross intact membrane of live cells and stains the nucleus of the live cells as light blue, wherein the apoptotic cell nuclei appears as bright blue due to chromatin condensation. Thus, it was of our interest to examine nuclear fragmentation or chromatin condensation induced by compounds **11c** and **11f**. For this, PC-3 cells were stained with DAPI following the treatment with both the compound **11c**, **11f** and cells were observed under fluorescence microscope for nuclear morphological changes. The results from Fig. 8 indicate that the nuclear structure of untreated cells was intact while **11c** and **11f** treated cells showed nuclear shrinkage, fragmented, pyknotic and horse shoe shaped nuclei (white arrow) and chromatin condensation, these are the remarkable features of apoptosis. These findings demonstrate that these compounds could induce apoptosis in PC-3 cells.

2.2.3.3. Effect of compounds 11c and 11d on mitochondrial membrane potential (DΨm). The maintenance of mitochondrial membrane potential (DΨm) is essential for mitochondrial integrity and cellular bioenergetic functions. During drug-induced apoptosis, a mitochondrial change such as loss of mitochondrial membrane potential (DΨm) is the key event that usually takes place. It is reported that collapse of mitochondrial membrane potential can be correlated to the early events that appear during the apoptotic process. Mitochondrial injury by compounds **11c** and **11f** was assessed based on the loss of mitochondrial membrane potential (DΨm) as indicated by green to red fluorescence ratio [46]. It was determined by using spectrofluorometer with JC-1, a cell permeable cationic, tracer dye that emits green and red fluorescence based on the membrane potential of mitochondria. In cells with healthy mitochondria, JC-1 accumulates in mitochondria and forms JC-1 oligomers that exhibit red fluorescence. However, JC-1 remains as monomers which emit green fluorescence in the depolarized mitochondria containing cells. Spectrofluorimetric analysis of PC-3 cells after treatment with 5 μM of **11c** and **11f** disclosed that both the compounds significantly increased green/red fluorescence ratio from 0.103 (control) to 0.135 (**11c**), 0.132 (**11f**) (Fig. 9). These results prove the collapse of mitochondrial membrane potential by the compounds **11c** and **11f** and suggest the involvement of mitochondria dependent pathway in their mechanism of action.

2.2.4. Flow-cytometry analysis

Cytotoxic agents usually alter the regulation of cell cycle resulting in the arrest of cell division in various phases, thereby prevents the growth and proliferation of cancer cells. The screening

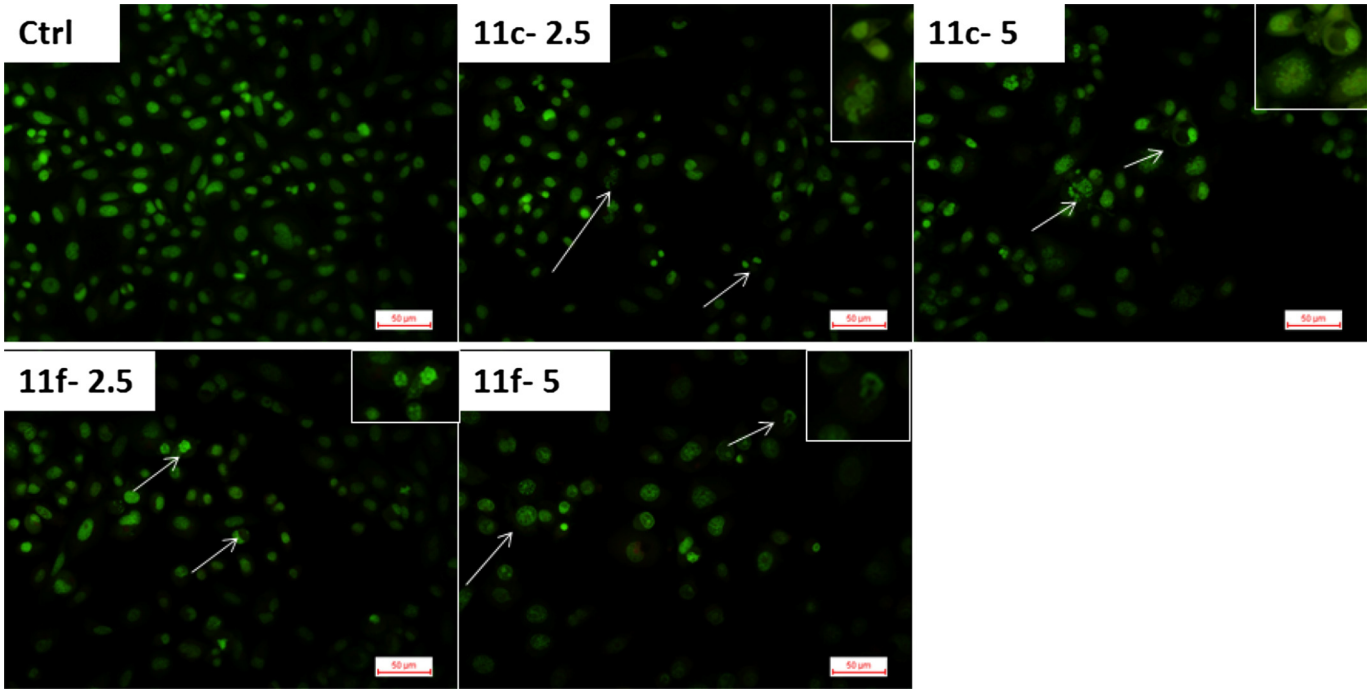

Fig. 7. Morphological changes in PC-3 cells treated with and without compound **11c** and **11f** for 48 h. Green live cells show normal morphology of control and early signs of apoptosis such as extremely condensed chromatin, horse-shoe shaped nuclei and destructive fragmentation of the nuclei were clearly observed in **11c** and **11f** treated cells at indicated concentrations. (For interpretation of the references to colour in this figure legend, the reader is referred to the web version of this article.)

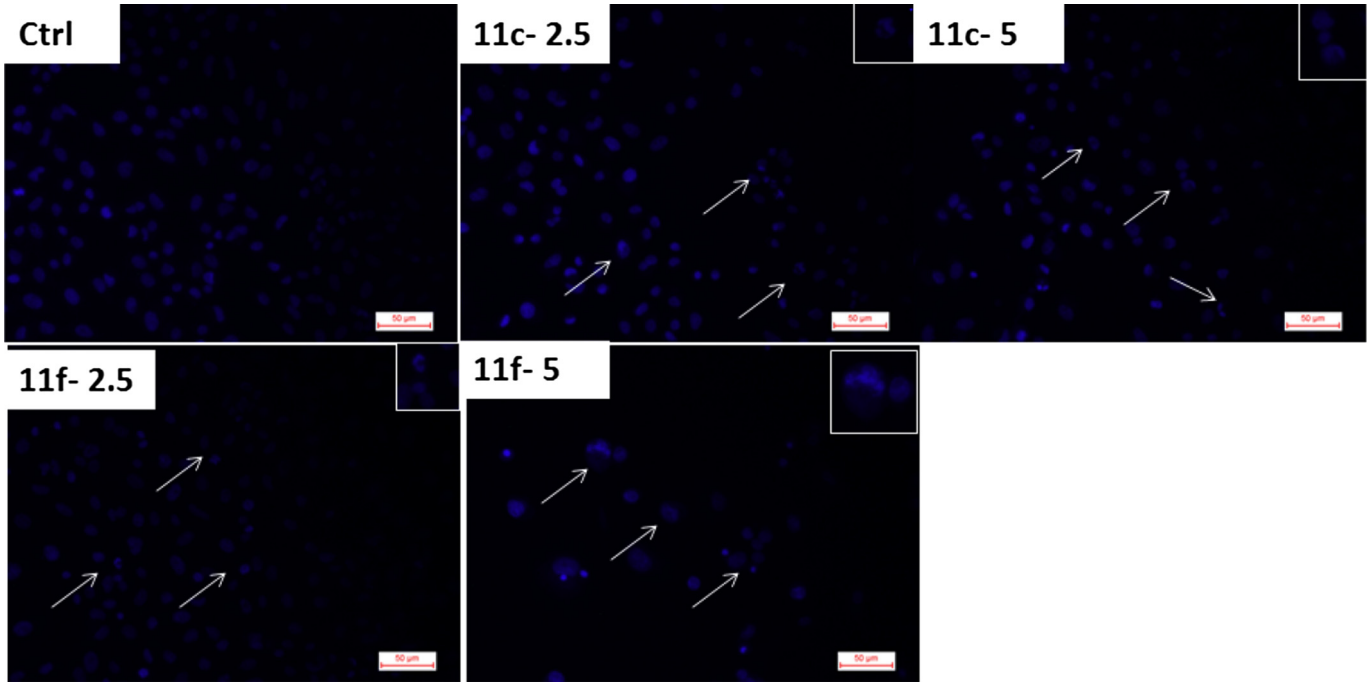

Fig. 8. Compounds **11c** and **11f** induced nuclear morphological changes in PC-3 cells after treatment for 48h.

results revealed that **11c** could exhibit significant antiproliferative activity on PC-3 cells. To understand whether this inhibition of growth of PC-3 cells is on account of cell cycle arrest, cell cycle distribution of PC-3 cells was determined by flow-cytometry analysis [47]. PC-3 cells were treated with **11c** at 2.5, 5 μM and **11f** at 2.5, 5, 10 μM and stained with propidium iodide, which was analyzed further by using flow cytometer (FACS verse, Becton Dickinson, US). The results from Fig. 10 demonstrate that the control cells showed 12.2% cells in G2/M phase, while the treatment with **11c** resulted in the increase of G2/M population to 57.5% (at 2.5 μM) in 24 h. Treatment with **11f** at 2.5, 5 and 10 μM displayed rise in G2/M population from 24.74% (control) to 27.04%, 29.87% and 31.42% respectively. These findings clearly indicate that the treatment of PC-3 cells with **11c** results in G2/M cell cycle arrest.

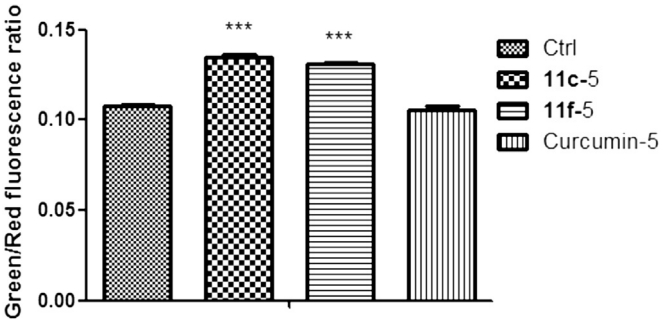

Fig. 9. Effect of compounds **11c** and **11f** on mitochondrial membrane potential (ΔΨm). The compound treated PC-3 cells were stained with JC-1 and the intensity of red and green fluorescence in each sample was analyzed by spectroflourometer. Data were mean ± SEM of three independent experiments.*P < 0.05 when compared to control (One way ANNOVA followed by Dunnet's multiple comparison test).

However, the % inhibition of cell cycle at G2/M phase is less for the compound **11f** when compared to **11c**.

2.3. Molecular modelling studies

Molecular modelling studies were performed extensively on tubulin (PDB code: 3E22) [48] to gain better understanding on the potency of the studied compounds (**11c** and **11f**) and to support the discussion of the biological results obtained in the previous sections. As the active site, at which colchicine binds, is located at the interface of α,β-tubulin subunits, both the α and β chains have been considered for molecular modelling studies [49]. Fig. 11 shows the binding of **11c** and **11f** at the interface (colchicine binding site of tubulin) of α,β-tubulin subunits. The significant hydrogen bonding interactions are shown as yellow dotted lines and the amino acid residues that interact with ligands are highlighted as shown in Fig. 11.

The promising compounds (**11c** and **11f**) were docked in a similar fashion at the active site and sandwiched between the amino acid residues like αAsn101, αSer178, αThr179, αAla180, αVal181, αArg221, αTyr224 of α-chain and βLys254, βLeu255, βAsn258, βMet259, βVal315, βThr353 and βAla354 of β-chain of tubulin. Compound **11c** showed significant hydrogen bond interaction between one of the hydrogens of $CONH_2$ group of αAsn101 and carbonyl oxygen of penta-1,4-dien-3-one linear linker (H ….O) at a distance of 2.38 Å. In addition, one more hydrogen bond was observed between carbonyl oxygen of βThr353 and NH hydrogen of indole ring (O ….H) at a distance of 2.13 Å. Moreover, some of the hydrophobic interactions were also observed between the ligand and αVal181, βLeu255, and βLys254. Compound **11f** was also docked in a similar fashion at the interface of two chains and showed a strong hydrogen bond interaction between carbonyl oxygen of COOH group of αGlu71 and NH hydrogen of indole ring (O ….H) at a distance of 1.92 Å while the other surrounded amino acid residues such as βLeu248, βAsn258, βLeu255 and βAla250 experienced hydrophobic contacts. However the indole ring and carbonyl oxygen of linear linker played a significant role in showing the hydrogen bond interactions with the amino acid residues, whereas the phenyl rings of both the conjugates were burried at the hydrophobic region. The linear linker also played a bridging role between the phenyl and indole rings, that leads to a successful docking at the target binding site (Fig. 12) suggesting that **11f** and **11c** are potent inhibitors of tubulin. To gain further insight of our findings, we demonstrated the superimposition of colchicine with the ligands and the corresponding superimposition poses suggest that methoxy phenyl ring of ligands under investigation occupied similar position with respect to 2-methoxycyclohepta-2,4,6-trien-1-one ring of colchicine and the carbonyl group in **11c** superimposes with the amide carbonyl of the colchicine as seen in Fig. 12.

3. Conclusion

In summary, a series of curcumin inspired indole analogues were synthesized, and evaluated for their anticancer potential. An initial screening was performed against lung (A549), breast (MDA-MB-231, BT549 and 4T1), prostate (PC-3, DU145), gastric (HGC-27) and cervical (HeLa) cancer cell lines by using MTT assay. Interestingly, compounds **11c** (1E, 4E)-1-(2,5-dimethoxyphenyl)-5-(1H-indol-3-yl)penta-1,4-dien-3-one and **11f** (1E, 4E)-1-(3,4,5-trimethoxyphenyl)-5-(1H-indol-3-yl)penta-1,4-dien-3-one showed the most potent antiproliferative activity on PC-3 cell lines (IC_{50} of 6.34 ± 0.25 and 3.15 ± 1.91 μM respectively). Most importantly, these compounds were found to be safe towards normal prostate epithelial cells (RWPE-1) compared to PC-3 cell line. Both **11c** and **11f** effectively inhibited the polymerization of tubulin with IC_{50} values 10.21 ± 0.10 and 8.83 ± 0.06 μM respectively. Molecular modelling studies suggest that **11c** and **11f** bind at the colchicine binding site of the tubulin. The detailed studies like AO/EB staining and DAPI nuclear staining suggest that the cell proliferation is inhibited through induction of apoptosis. In addition, the treatment with **11c** and **11f** results in the collapse of mitochondrial membrane potential in PC-3 cells. The flow-cytometry analysis confirmed the arrest of PC-3 cells in the G2/M phase of cell cycle by **11c** whereas **11f** showed modertae increase in the G2/M population. Overall, the current studies demonstrate that curcumin inspired indole analogues like **11c** and **11f** have the potential to be developed as leads and their further structural modifications may produce promising new cancer therapeutics.

4. Experimental section

4.1. General

All solvents were purified and dried using standard methods prior to use. Commercially available reagents were used without further purification. The reactions were monitored by thin layer chromatography (TLC), using MERCK pre-coated silica gel 60-F_{254} aluminum plates. Visualization of spots on TLC plates was done by UV light. Column chromatography with 60–120 mesh silica gel was used as separation and purification method. Ethyl acetate and hexane were used as eluent. Melting points were obtained on Stuart digital melting-point apparatus/SMP 30 and were uncorrected. All IR spectra were recorded on a Perkin Elmer, FT-IR spectrometer using KBr discs. ^{1}H NMR spectra were recorded on an Avance NMR instrument operated at 500 MHz. ^{13}C NMR spectra were recorded on an Avance NMR instrument operated at 125 MHz. Chemical shift values were reported in ppm with TMS as an internal reference and *J* values were given in Hertz. The following abbreviations were used for ^{1}H NMR spectra to indicate the signal multiplicity: s (singlet), d (doublet), t (triplet), q (quartet) and m (multiplet). HRMS were determined with Agilent QTOF mass spectrometer 6540 series instrument and were performed in the ESI techniques at 70 eV.

4.2. Synthetic procedures and spectral data

4.2.1. General synthetic procedure for the synthesis of *2*

To a magnetically stirred solution of an appropriately substituted benzaldehyde **1** (1 mmol) in methanol (5 mL) was added sodium borohydride (2 mmol) slowly over 10 min at 0 °C. The resulting solution was stirred at room temperature for the

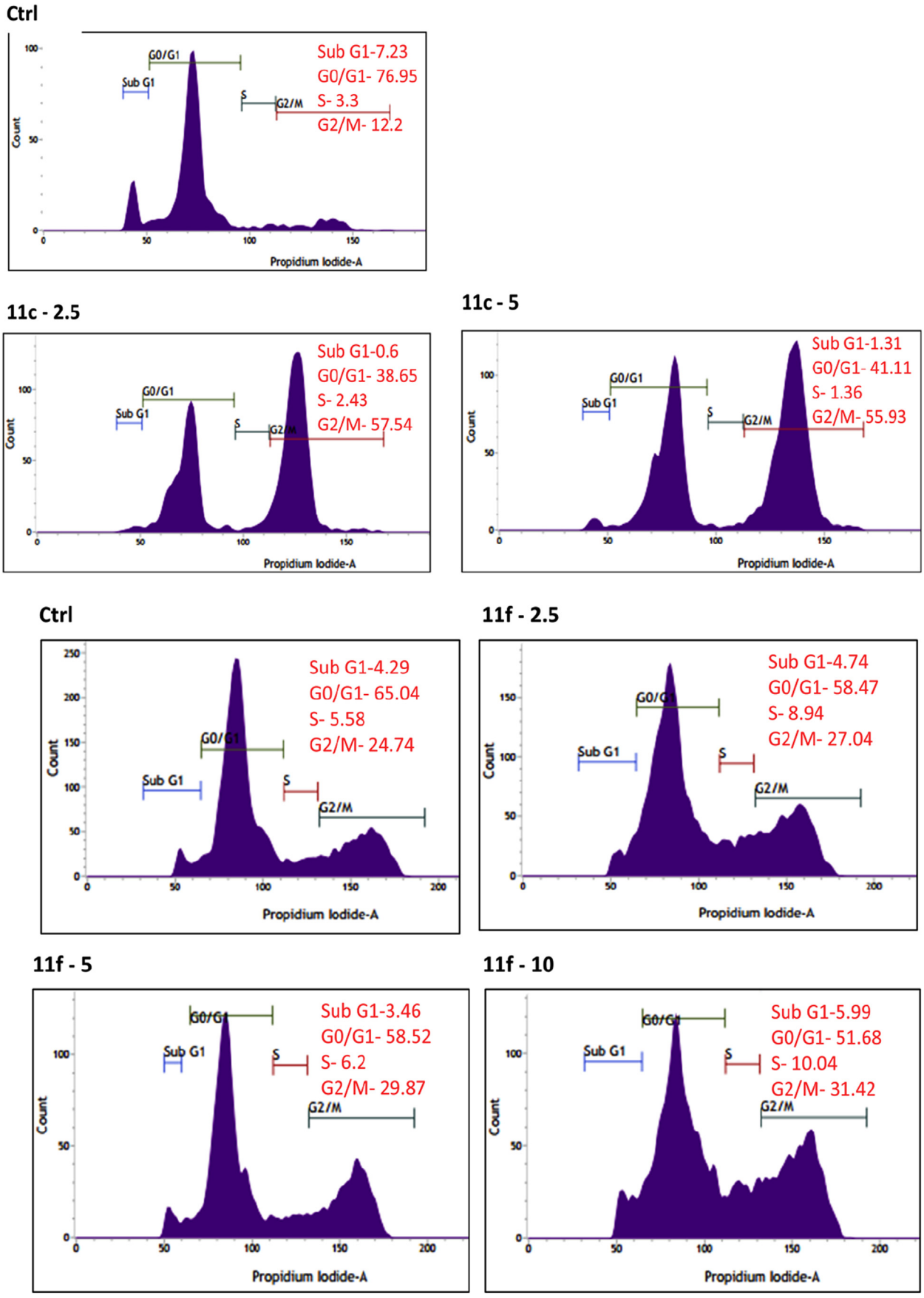

Fig. 10. Effect of compounds **11c** and **11f** on cell cycle progression of PC-3 cells. Cells were treated with compounds **11c** and **11f** for 24 h followed by analysis of cell cycle distribution using propidium iodide cell staining method. All assays were done in triplicate.

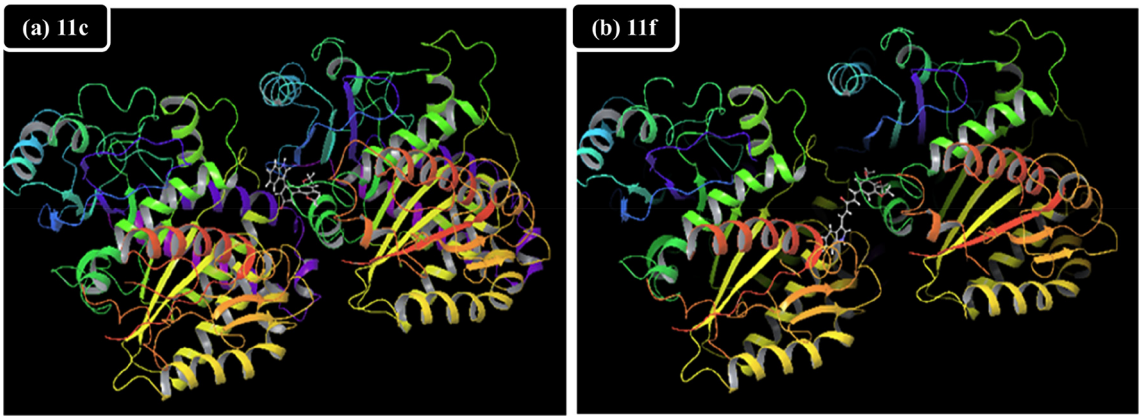

Fig. 11. Poses represent the binding of compounds **11c** and **11f** at the interface of α,β-tubulin subunits (colchicine binding site of tubulin).

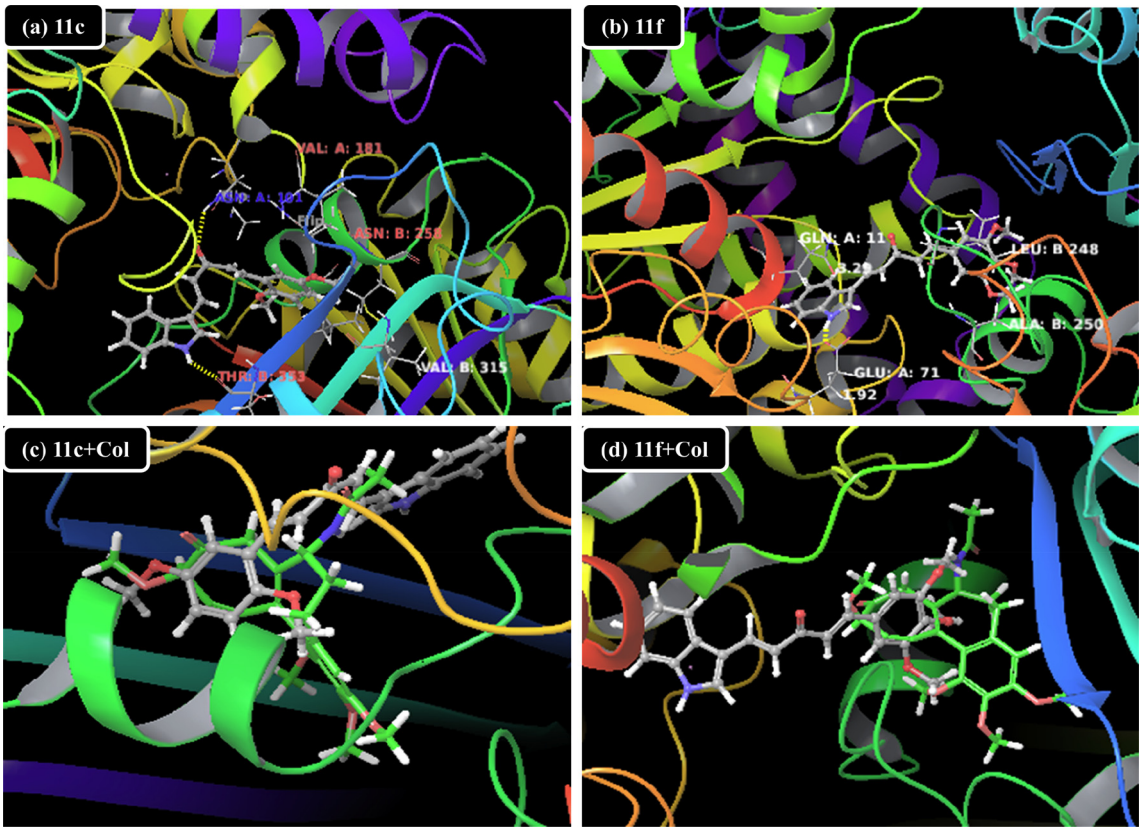

Fig. 12. **(a)**, **(b)** Docking poses of ligands **11c**, **11f** respectively and the interacting amino acids at the colchicine binding domain of tubulin. **(c)**, **(d)** Poses represent the superimposition of potential ligands (**11c** and **11f**) and colchicine at the colchicine binding domain: The potential ligands were shown as ball and stick model, while the interacting amino acids were denoted as thin tubes and the colchicine was shown as green ball and stick model in the black background. (For interpretation of the references to colour in this figure legend, the reader is referred to the web version of this article.)

required time. On completion, the reaction mixture was quenched with 3% aqueous HCl solution, and evaporated to dryness. The residue was extracted with CH_2Cl_2, dried over Na_2SO_4 and concentrated under vaccum to obtain corresponding alcohol **2** which was used without further purification.

*4.2.2. General synthetic procedure for the synthesis of **3***

To a stirred solution of alcohol **2** (1 mmol) in dry ether (10 mL) was added phosphorus tribromide (0.5 mL) dropwise at 0 °C and the reaction mixture was stirred for 0.5 h. After completion of the reaction (TLC monitoring), the reaction mixture was carefully poured over ice, and the aqueous phase was extracted with ether. The combined organic layers were washed with $NaHCO_3$ and water, followed by brine. Drying over Na_2SO_4 and evaporation of the solvents under reduced pressure affords the desired benzyl bromide **3** which was used without further purification.

*4.2.3. General procedure for the synthesis of **5a-f***

To a suspension of NaH 60% in oil (2.25 mmol) in dry DMF (0.8 mL/mmol) was added, at 0 °C and under nitrogen atmosphere, a solution of indole-3-carboxaldehyde **4** (1 mmol) in dry DMF (2.5 mL/mmol). After stirring for 30 min at room temperature, benzyl bromide **3** (1.2 mmol) was slowly added. On completion, the reaction was quenched by addition of water and the product was extracted with diethyl ether. The organic layer was dried over Na_2SO_4, filtered off and concentrated under vacuum. The crude residue was purified by column chromatography (Silica gel, 60–120 mesh, 9:1 hexane/ethyl acetate) to obtain the desired aldehyde **5a-f**.

*4.2.4. General procedure for the synthesis of **8a-f***

To a stirred solution of benzaldehyde **6** (1 mmol) in ethanol (3 mL) was added 0.5 mL of acetone and 15% aqueous NaOH (1 mL) solution at 0 °C. The reaction was allowed to stir at room temperature till it was completed. The reaction mixture was evaporated to dryness, extracted twice with ethyl acetate, the combined organic layers were dried over anhydrous Na_2SO_4 and concentrated under reduced pressure. The crude product was purified by column chromatography (Silica gel, 60–120 mesh, 9:1 hexane/ethyl acetate) to obtain the desired chalcone **8a-f**.

*4.2.5. Procedure for the synthesis of **8g***

Similarly, to a stirred solution of indole-3-carboxaldehyde **4** (1 mmol) in ethanol (5 mL) was added 0.5 mL of acetone and 15% aqueous NaOH (3 mL) solution at 0 °C. The reaction was allowed to stir at room temperature till it was completed. The reaction mixture was evaporated to dryness and similar work up procedure as described for chalcones **8a-f** was followed to extract the compound from reaction mixture. Further, it was purified by column chromatography (Silica gel, 60–120 mesh, 9:1 hexane/ethyl acetate) to obtain pure chalcone **8g**.

*4.2.6. General procedure for the synthesis of **9a-s***

To a stirred solution of chalcone **8a-f** (0.5 mmol) in ethanol (3 mL) was added 15% aqueous NaOH (1 mL) solution and aldehyde **5** (0.5 mmol) at 0 °C. The resulting solution was stirred at room temperature till the completion of the reaction. The reaction mixture was evaporated to dryness, extracted twice with ethyl acetate, the combined organic layers were dried over anhydrous Na_2SO_4 and concentrated under reduced pressure. The crude mass was purified by column chromatography (Silica gel, 60–120 mesh, 8:2 hexane/ethyl acetate) to give the pure product **9a-s**.

*4.2.7. General procedure for the synthesis of **11a-f***

To a stirred solution of chalcone **8g** (0.5 mmol) in ethanol (5 mL) was added 15% aqueous NaOH (2 mL) solution and aldehyde **10** (0.5 mmol) at 0 °C. The resulting solution was stirred at room temperature till the completion of the reaction. The reaction mixture was evaporated to dryness, extracted twice with ethyl acetate, the combined organic layers were dried over anhydrous Na_2SO_4 and concentrated under reduced pressure. The crude mass was purified by column chromatography (Silica gel, 60–120 mesh, 3:2 hexane/ethyl acetate) to give the pure product **11a-f**.

4.2.8. Spectral data

*4.2.8.1. (1E,4E)-1-(1-benzyl-1H-indol-3-yl)-5-(4-chlorophenyl) penta-1,4-dien-3-one (**9a**).* Yellow solid, yield 75.3%; mp: 136–138 °C; IR (KBr, cm^{-1}): 3092.9, 2922.0, 1658.8, 1619.4, 1385.0, 974.8; ^{1}H NMR (500 MHz, $CDCl_3$): δ 8.11–7.97 (m, 1H), 7.76–7.66 (m, 1H), 7.59–7.50 (m, 2H), 7.45–7.29 (m, 6H), 7.22–6.78 (m, 6H), 5.36 (s, 2H); ^{13}C NMR (125 MHz, $CDCl_3$): δ 188.6, 142.1, 140.4, 137.8, 136.5, 135.9, 133.8, 133.2, 129.5, 129.3, 129.1, 128.2, 127.0, 126.5, 125.7, 123.4, 121.8, 121.2, 120.9, 113.3, 110.7, 50.6; HRMS (ESI): *m/z* calcd for $C_{26}H_{21}ClNO$ 398.1306, found 398.1309 $[M+H]^+$.

*4.2.8.2. (1E,4E)-1-(1-benzyl-1H-indol-3-yl)-5-(4-methoxyphenyl) penta-1,4-dien-3-one (**9b**).* Yellow solid, yield 78.4%; mp: 140–142 °C; IR (KBr, cm^{-1}): 3109.2, 2988.5, 1660.5, 1612.4, 1390.0, 980.3; ^{1}H NMR (500 MHz, $CDCl_3$): δ 8.09–7.95 (m, 2H), 7.71 (d, J = 15.8 Hz, 1H), 7.59 (d, J = 8.7 Hz, 2H), 7.51 (s, 1H), 7.41–7.27 (m, 6H), 7.16 (d, J = 6.8 Hz, 2H), 7.09 (d, J = 15.8 Hz, 1H), 6.99 (d, J = 15.8 Hz, 1H), 6.94 (d, J = 8.7 Hz, 2H), 5.35 (s, 2H), 3.86 (s, 3H); ^{13}C NMR (125 MHz, $CDCl_3$): δ 188.9, 161.3, 141.7, 137.8, 136.6, 136.0, 133.3, 129.9, 129.0, 128.1, 127.9, 127.0, 126.4, 124.0, 123.2, 121.6, 121.5, 120.9, 114.3, 113.4, 110.6, 55.4, 50.5; HRMS (ESI): *m/z* calcd for $C_{27}H_{24}NO_2$ 394.1802, found 394.1770 $[M+H]^+$.

*4.2.8.3. (1E,4E)-1-(1-(4-chlorobenzyl)-1H-indol-3-yl)-5-(4-methoxyphenyl)penta-1,4-dien-3-one (**9c**).* Yellow solid, yield 74.8%; mp: 134–136 °C; IR (KBr, cm^{-1}): 3097.4, 2959.4, 1656.3, 1621.1, 1395.0, 1170.2, 974.9, 836.1; ^{1}H NMR (500 MHz, $CDCl_3$): δ 8.15–7.93 (m, 2H), 7.74 (d, J = 15.7 Hz, 1H), 7.66–7.56 (m, 2H), 7.51 (s, 1H), 7.38–7.28 (m, 4H), 7.20–6.87 (m, 7H), 5.33 (s, 2H), 3.87 (s, 3H); ^{13}C NMR (125 MHz, $CDCl_3$): δ 188.9, 161.3, 141.9, 137.6, 136.4, 134.6, 134.0, 133.1, 133.0, 129.2, 128.2, 127.9, 126.4, 124.0, 123.4, 121.8, 121.7, 120.9, 114.3, 113.6, 110.5, 55.4, 49.9; HRMS (ESI): *m/z* calcd for $C_{27}H_{23}ClNO_2$ 428.1412, found 428.1413 $[M+H]^+$.

*4.2.8.4. (1E,4E)-1-(1-(3-fluorobenzyl)-1H-indol-3-yl)-5-(4-methoxyphenyl)penta-1,4-dien-3-one (**9d**).* Yellow solid, yield 78.1%; mp: 164–166 °C; IR (KBr, cm^{-1}): 3093.6, 3002.3, 1657.3, 1620.9, 1394.4, 1253.5, 1107.5, 966.2; ^{1}H NMR (500 MHz, $CDCl_3$): δ 8.12–7.99 (m, 2H), 7.74 (d, J = 15.8, 1H), 7.61 (d, J = 8.5 Hz, 2H), 7.53 (s, 1H), 7.37–7.29 (m, 4H), 7.13 (d, J = 15.8 Hz, 1H), 7.07–6.92 (m, 5H), 6.86 (d, J = 9.3 Hz, 1H), 5.35 (s, 2H), 3.87 (s, 3H); ^{13}C NMR (125 MHz, $CDCl_3$): δ 188.8, 164.1, 162.2, 161.2, 141.9, 138.7, 137.6, 136.4, 133.1, 130.6, 130.0, 127.9, 126.4, 124.0, 123.4, 122.4, 121.8, 121.7, 120.9, 115.1, 114.3, 113.8, 110.4, 55.4, 50.0; HRMS (ESI): *m/z* calcd for $C_{27}H_{23}FNO_2$ 412.1707, found 412.1710 $[M+H]^+$.

*4.2.8.5. (1E,4E)-1-(1-(4-fluorobenzyl)-1H-indol-3-yl)-5-(4-methoxyphenyl)penta-1,4-dien-3-one (**9e**).* Yellow solid, yield 76.3%; mp: 153–154 °C; IR (KBr, cm^{-1}): 3096.5, 3003.0, 1656.6, 1617.9, 1381.2, 1169.8, 1102.3, 971.9; ^{1}H NMR (500 MHz, $CDCl_3$): δ 8.07–7.95 (m, 2H), 7.72 (d, J = 15.8 Hz, 1H), 7.59 (d, J = 8.6 Hz, 2H), 7.49 (s, 1H), 7.35–7.27 (m, 3H), 7.17–6.90 (m, 8H), 5.31 (s, 2H), 3.86 (s, 3H); ^{13}C NMR (125 MHz, $CDCl_3$): δ 184.1, 158.7, 156.6, 137.1, 132.9, 131.7, 128.3, 127.0, 125.2, 124.0, 123.1, 121.7, 119.2, 118.6, 116.9, 116.2, 111.3, 111.1, 109.6, 108.8, 106.7, 50.0, 45.1; HRMS (ESI): *m/z* calcd for $C_{27}H_{23}FNO_2$ 412.1707, found 412.1709 $[M+H]^+$.

*4.2.8.6. (1E,4E)-1-(4-methoxyphenyl)-5-(1-(4-(trifluoromethyl) benzyl)-1H-indol-3-yl)penta-1,4-dien-3-one (**9f**).* Yellow solid, yield 74.2%; mp: 148–150 °C; IR (KBr, cm^{-1}): 3097.1, 2969.8, 1644.9, 1597.9, 1323.6, 1168.9, 1109.2, 976.4; ^{1}H NMR (500 MHz, $CDCl_3$): δ 8.07–7.97 (m, 2H), 7.72 (d, 1H, J = 15.8), 7.62–7.55 (m, 4H), 7.52 (s, 1H), 7.34–7.26 (m, 3H), 7.25–7.21 (m, 2H), 7.12 (d, J = 15.8 Hz, 1H), 6.99 (d, J = 15.8 Hz, 1H), 6.94 (d, J = 8.6 Hz, 2H), 5.41 (s, 2H), 3.85 (s, 3H); ^{13}C NMR (125 MHz, $CDCl_3$): δ 188.9, 161.4, 142.0, 140.2, 137.6, 136.3, 133.0, 130.0, 127.8, 127.0, 126.5, 126.0, 124.0, 123.5, 122.0, 121.8, 121.0, 114.4, 113.8, 110.3, 55.4, 50.0; HRMS (ESI): *m/z* calcd for $C_{28}H_{23}F_3NO_2$ 462.1675, found 462.1673 $[M+H]^+$.

*4.2.8.7. (1E,4E)-1-(1-benzyl-1H-indol-3-yl)-5-(2,5-dimethoxyphenyl)penta-1,4-dien-3-one (**9g**).* Yellow solid, yield 81.2%; mp: 154–156 °C; IR (KBr, cm^{-1}): 3094.2, 2988.7, 1662.0, 1612.1, 1383.0, 1100.2, 984.2; ^{1}H NMR (500 MHz, $CDCl_3$): δ 8.12–7.98

(m, 3H), 7.54 (s, 1H), 7.38–7.29 (m, 6H), 7.20–7.11 (m, 5H), 6.97–6.92 (m, 2H), 5.37 (s, 2H), 3.90 (s, 3H), 3.85 (s, 3H); ^{13}C NMR (125 MHz, $CDCl_3$): δ 189.3, 153.5, 153.0, 137.7, 137.0, 136.7, 136.0, 133.2, 128.9, 128.1, 127.1, 126.9, 126.4, 124.7, 123.2, 121.5, 121.3, 120.8, 116.9, 113.3, 113.0, 112.4, 110.5, 56.1, 55.8, 50.5; HRMS (ESI): *m/z* calcd for $C_{28}H_{26}NO_3$ 424.1907, found 424.1928 $[M+H]^+$.

*4.2.8.8. (1E,4E)-1-(2,5-dimethoxyphenyl)-5-(1-(4-fluorobenzyl)-1H-indol-3-yl)penta-1,4-dien-3-one (**9h**).* Yellow solid, yield 78.6%; mp: 152–154 °C; IR (KBr, cm^{-1}): 3095.8, 2956.8, 1662.6, 1644.6, 1347.8, 1218.0, 1107.7, 984.4;^{1}H NMR (500 MHz, $CDCl_3$): δ 8.07–7.96 (m, 3H), 7.49 (s, 1H), 7.33–7.30 (m, 3H), 7.19–7.08 (m, 5H), 7.05–6.99 (m, 2H), 6.94–6.85 (m, 2H), 5.31 (s, 2H), 3.88 (s, 3H), 3.82 (s, 3H); ^{13}C NMR (125 MHz, $CDCl_3$): δ 189.3, 163.4, 161.4, 153.5, 153.0, 137.6, 137.1, 136.5, 132.9, 131.8, 128.6, 127.1, 126.5, 124.7, 123.3, 121.5, 120.9, 117.0, 115.9, 113.5, 113.0, 112.4, 110.4, 56.1, 55.8, 49.8; HRMS (ESI): *m/z* calcd for $C_{28}H_{25}FNO_3$ 442.1813, found 442.1804 $[M+H]^+$.

*4.2.8.9. (1E,4E)-1-(2,5-dimethoxyphenyl)-5-(1-(4-(trifluoromethyl) benzyl)-1H-indol-3-yl)penta-1,4-dien-3-one (**9i**).* Yellow solid, yield 75.4%; mp: 181–183 °C; IR (KBr, cm^{-1}): 3097.1, 2988.6, 1662.9, 1610.1, 1325.0, 1177.2, 1106.6, 984.3; ^{1}H NMR (500 MHz, $CDCl_3$): δ 8.132–7.95 (m, 3H), 7.58 (d, *J* = 7.9 Hz, 2H), 7.52 (s, 1H), 7.48–7.27 (m, 3H), 7.25–7.08 (m, 5H), 6.96–6.85 (m, 2H), 5.41 (s, 2H), 3.88 (s, 3H), 3.82 (s, 3H); ^{13}C NMR (125 MHz, $CDCl_3$): δ 189.3, 153.5, 153.1, 140.2, 137.5, 137.2, 136.3, 132.9, 130.4, 127.1, 127.0, 126.5, 126.0, 124.7, 123.5, 121.7, 121.0, 117.0, 113.8, 113.1, 112.5, 110.4, 56.1, 55.8, 50.0; HRMS (ESI): *m/z* calcd for $C_{29}H_{25}F_3NO_3$ 492.1781, found 492.1815 $[M+H]^+$.

*4.2.8.10. (1E,4E)-1-(3,4-dimethoxyphenyl)-5-(1-(4-fluorobenzyl)-1H-indol-3-yl)penta-1,4-dien-3-one (**9j**).* Yellow solid, yield 73.5%; mp: 177–178 °C; IR (KBr, cm^{-1}): 3095.2, 2989.1, 1657.6, 1616.9, 1380.0, 1253.0, 1133.7, 972.1; ^{1}H NMR (500 MHz, $CDCl_3$): δ 8.09–7.96 (m, 2H), 7.71 (d, *J* = 15.8 Hz, 1H), 7.50 (s, 1H), 7.36–7.28 (m, 3H), 7.25–6.93 (m, 8H), 6.91 (d, *J* = 8.3 Hz, 1H), 5.32 (s, 2H), 3.97 (s, 3H), 3.94 (s, 3H); ^{13}C NMR (125 MHz, $CDCl_3$): δ 188.7, 163.4, 161.4, 151.0, 149.2, 142.0, 137.6, 136.5, 133.1, 131.7, 128.6, 128.1, 126.4, 124.3, 123.3, 122.9, 121.5, 120.9, 115.9, 113.5, 111.0, 110.4, 109.8, 55.9, 49.8; HRMS (ESI): *m/z* calcd for $C_{28}H_{25}FNO_3$ 442.1813, found 442.1804 $[M+H]^+$.

*4.2.8.11. (1E,4E)-1-(1-benzyl-1H-indol-3-yl)-5-(2,4,5-trimethoxyphenyl)penta-1,4-dien-3-one (**9k**).* Yellow solid, yield 82.1%; mp: 174–176 °C; IR (KBr, cm^{-1}): 3096.9, 2962.8, 1661.5, 1602.3, 1389.1, 1099.4, 985.2; ^{1}H NMR (500 MHz, $CDCl_3$): δ 8.11–7.94 (m, 3H), 7.50 (s, 1H), 7.38–7.26 (m, 6H), 7.20–7.11 (m, 4H), 6.91 (d, *J* = 16 Hz, 1H), 6.53 (s, 1H), 5.34 (s, 2H), 3.94 (s, 3H), 3.91 (s, 6H); ^{13}C NMR (125 MHz, $CDCl_3$): δ 189.3, 154.2, 152.1, 143.3, 137.7, 136.9, 136.2, 136.1, 133.1, 128.9, 128.0, 127.0, 126.5, 124.7, 123.2, 121.4, 120.8, 115.7, 113.4, 110.8, 110.5, 96.9, 56.4, 56.0, 50.5; HRMS (ESI): *m/z* calcd for $C_{29}H_{28}NO_4$ 454.2013, found 454.2057 $[M+H]^+$.

*4.2.8.12. (1E,4E)-1-(1-(4-fluorobenzyl)-1H-indol-3-yl)-5-(2,4,5-trimethoxyphenyl)penta-1,4-dien-3-one (**9l**).* Yellow solid, yield 84.3%; mp: 170–172 °C; IR (KBr, cm^{-1}): 3097.1, 2988.6, 1658.8, 1600.5, 1387.7, 1209.3, 1092.3, 982.4; ^{1}H NMR (500 MHz, $CDCl_3$): δ 8.13–7.91 (m, 3H), 7.48 (s, 1H), 7.32–7.24 (m, 3H), 7.20–6.90 (m, 7H), 6.52 (s, 1H), 5.30 (s, 2H), 3.94 (s, 3H), 3.90 (s, 6H); ^{13}C NMR (125 MHz, $CDCl_3$): δ 189.2, 163.3, 161.4, 154.1, 152.1, 143.3, 137.5, 137.0, 136.0, 132.8, 131.8, 128.6, 126.4, 124.6, 123.2, 121.5, 120.9, 116.0, 115.8, 115.6, 113.5, 110.7, 110.4, 96.9, 56.5, 56.4, 56.0, 49.7; HRMS (ESI): *m/z* calcd for $C_{29}H_{27}FNO_4$ 472.1919, found 472.1957 $[M+H]^+$.

*4.2.8.13. (1E,4E)-1-(1-(4-(trifluoromethyl)benzyl)-1H-indol-3-yl)-5-(2,4,5-trimethoxyphenyl)penta-1,4-dien-3-one (**9m**).* Yellow solid, yield 79.5%; mp: 214–216 °C IR (KBr, cm^{-1}): 3109.2, 2988.5, 1660.5, 1604.5, 1325.8, 1285.5, 1087.0, 980.3; ^{1}H NMR (500 MHz, $CDCl_3$): δ 8.11–7.98 (m, 3H), 7.63–7.50 (m, 3H), 7.36–7.27 (m, 4H), 7.24–7.12 (m, 3H), 7.00 (d, *J* = 16 Hz, 1H), 6.53 (s, 1H), 5.42 (s, 2H), 3.95 (s, 3H), 3.92 (s, 3H), 3.91 (s, 3H); ^{13}C NMR (125 MHz, $CDCl_3$): δ 189.2, 154.2, 152.1, 143.3, 140.2, 137.5, 137.1, 135.8, 132.7, 130.4, 130.2, 126.9, 126.5, 125.9, 124.6, 123.4, 121.7, 121.0, 115.6, 113.8, 110.7, 110.3, 96.8, 56.4, 56.0, 49.9; HRMS (ESI): *m/z* calcd for $C_{30}H_{27}F_3NO_4$ 522.1887, found 522.1906 $[M+H]^+$.

*4.2.8.14. (1E,4E)-1-(1-benzyl-1H-indol-3-yl)-5-(2,4,6-trimethoxyphenyl)penta-1,4-dien-3-one (**9n**).* Yellow solid, yield 79.3%; mp: 151–153 °C; IR (KBr, cm^{-1}): 3091.3, 2934.6, 2836.6, 1651.2, 1595.1, 1340.7, 1285.1, 1098.7, 972.5; ^{1}H NMR (500 MHz, $CDCl_3$): δ 8.19 (d, *J* = 16.1 Hz, 1H), 8.07–8.01 (m, 1H), 7.98 (d, *J* = 11.7 Hz, 1H), 7.48 (s, 1H), 7.42 (d, *J* = 16.1 Hz, 1H), 7.37–7.26 (m, 6H), 7.20–7.09 (m, 3H), 6.14 (s, 2H), 5.33 (s, 2H), 3.91 (s, 6H), 3.86 (s, 3H); ^{13}C NMR (125 MHz, $CDCl_3$): δ 190.7, 162.7, 161.4, 137.6, 136.2, 135.3, 133.4, 132.6, 128.9, 128.0, 126.9, 126.6, 126.5, 123.0, 122.2, 121.3, 120.8, 113.5, 110.4, 106.6, 90.5, 55.7, 55.3, 50.4; HRMS (ESI): *m/z* calcd for $C_{29}H_{28}NO_4$ 454.2013, found 454.2009 $[M+H]^+$.

*4.2.8.15. (1E,4E)-1-(1-(4-chlorobenzyl)-1H-indol-3-yl)-5-(2,4,6-trimethoxyphenyl)penta-1,4-dien-3-one (**9o**).* Yellow solid, yield 83.4%; mp: 143–145 °C; IR (KBr, cm^{-1}): 3096.0, 2971.2, 1651.8, 1596.3, 1324.1, 1213.0, 1157.7, 991.4; ^{1}H NMR (500 MHz, $CDCl_3$): δ 8.35–7.88 (m, 3H), 7.62–7.28 (m, 6H), 7.25–6.88 (m, 4H), 6.16 (s, 2H), 5.32 (s, 2H), 3.93 (s, 6H), 3.88 (s, 3H); ^{13}C NMR (125 MHz, $CDCl_3$): δ 190.7, 162.8, 161.5, 137.5, 135.1, 134.8, 133.9, 133.6, 132.4, 129.1, 128.2, 126.6, 123.2, 122.5, 121.4, 120.9, 113.8, 110.3, 106.5, 90.5, 55.8, 55.4, 49.8; HRMS (ESI): *m/z* calcd for $C_{29}H_{27}ClNO_4$ 488.1623, found 488.1629 $[M+H]^+$.

*4.2.8.16. (1E,4E)-1-(1-(3-fluorobenzyl)-1H-indol-3-yl)-5-(2,4,6-trimethoxyphenyl)penta-1,4-dien-3-one (**9p**).* Yellow solid, yield 81.0%; mp: 131–132 °C; IR (KBr, cm^{-1}): 3093.8, 2988.4, 1649.6, 1601.4, 1341.6, 1260.5, 1176.6, 975.0; ^{1}H NMR (500 MHz, $CDCl_3$): δ 8.43–8.13 (m, 3H), 7.66–7.27 (m, 6H), 7.21–6.78 (m, 4H), 6.16 (s, 2H), 5.34 (s, 2H), 3.93 (s, 6H), 3.87 (s, 3H); ^{13}C NMR (125 MHz, $CDCl_3$): δ 190.7, 164.1, 162.8, 162.1, 161.5, 138.9, 137.5, 135.6, 135.2, 133.6, 132.9, 132.5, 130.6, 126.5, 123.3, 123.2, 122.5, 122.3, 121.6, 121.4, 120.9, 115.0, 113.9, 110.3, 106.5, 90.5, 55.8, 55.4, 49.8; HRMS (ESI): *m/z* calcd for $C_{29}H_{27}FNO_4$ 472.1919, found 472.1919 $[M+H]^+$.

*4.2.8.17. (1E,4E)-1-(1-(4-fluorobenzyl)-1H-indol-3-yl)-5-(2,4,6-trimethoxyphenyl)penta-1,4-dien-3-one (**9q**).* Yellow solid, yield 82.1%; mp: 152–154 °C; IR (KBr, cm^{-1}): 2972.2, 2901.7, 1659.9, 1594.0, 1391.9, 1336.9, 977.9; ^{1}H NMR (500 MHz, $CDCl_3$): δ 8.38–7.81 (m, 3H), 7.72–7.27 (m, 5H), 7.25–6.75 (m, 5H), 6.14 (s, 2H), 5.30 (s, 2H), 3.91 (s, 6H), 3.86 (s, 3H); ^{13}C NMR (125 MHz, $CDCl_3$): δ 190.7, 163.3, 162.7, 161.4, 137.5, 135.2, 133.5, 132.4, 131.9, 128.6, 126.5, 123.1, 122.4, 121.3, 120.9, 115.8, 113.6, 110.3, 106.5, 90.5, 55.7, 55.3, 49.7; HRMS (ESI): *m/z* calcd for $C_{29}H_{27}FNO_4$ 472.1919, found 472.1898 $[M+H]^+$.

*4.2.8.18. (1E,4E)-1-(1-(4-(trifluoromethyl)benzyl)-1H-indol-3-yl)-5-(2,4,6-trimethoxyphenyl)penta-1,4-dien-3-one (**9r**).* Yellow solid, yield 78.6%; mp: 203–205 °C; IR (KBr, cm^{-1}): 3105.0, 2970.7, 1633.8, 1601.9, 1321.6, 1292.2, 992.7; ^{1}H NMR (500 MHz, $CDCl_3$): δ 8.19 (d, *J* = 16.1 Hz, 1H), 8.05 (d, *J* = 7.4 Hz, 1H), 7.97 (d, *J* = 15.8 Hz, 1H), 7.58 (d, *J* = 7.8 Hz, 2H), 7.50 (s, 1H), 7.42 (d, *J* = 16.1 Hz, 1H), 7.35–7.27 (m, 2H), 7.25–7.19 (m, 3H), 7.16 (d, *J* = 15.8 Hz, 1H), 6.14 (s, 2H), 5.40 (s, 2H), 3.91 (s, 6H), 3.86 (s, 3H); ^{13}C NMR (125 MHz,

$CDCl_3$): δ 190.6, 162.8, 161.5, 140.4, 137.4, 135.0, 133.6, 132.3, 126.9, 126.5, 125.9, 123.3, 122.7, 121.5, 121.0, 114.0, 110.2, 106.5, 90.5, 55.7, 55.3, 49.7; HRMS (ESI): *m/z* calcd for $C_{30}H_{27}F_3NO_4$ 522.1887, found 522.1870 $[M+H]^+$.

*4.2.8.19. (1E,4E)-1-(1-(4-(trifluoromethoxy)benzyl)-1H-indol-3-yl)-5-(3,4-dimethoxyphenyl)penta-1,4-dien-3-one (**9s**).* Yellow solid, yield 75.8%; mp: 132–134 °C; IR (KBr, cm^{-1}): 3100.7, 2922.9, 1712.8, 1669.0, 1635.9, 1396.7, 1249.2, 985.4; ^1H NMR (500 MHz, $CDCl_3$): δ 8.13–7.93 (m, 2H), 7.71 (d, *J* = 15.8 Hz, 1H), 7.51 (s, 1H), 7.38–7.27 (m, 3H), 7.23–7.10 (m, 6H), 6.97 (d, *J* = 15.8 Hz, 1H), 6.90 (d, *J* = 8.3 Hz, 1H), 5.35 (s, 2H), 3.96 (s, 3H), 3.93 (s, 3H); ^{13}C NMR (125 MHz, $CDCl_3$): δ 188.8, 151.1, 149.2, 148.9, 142.2, 137.6, 136.5, 134.8, 133.1, 128.2, 128.1, 126.4, 124.4, 123.5, 122.9, 121.8, 121.6, 121.5, 121.0, 113.7, 111.1, 110.4, 109.8, 56.0, 55.9, 49.7; HRMS (ESI): *m/z* calcd for $C_{29}H_{25}F_3NO_4$ 508.1730, found 508.1769 $[M+H]^+$.

*4.2.8.20. (1E,4E)-1-(4-chlorophenyl)-5-(1H-indol-3-yl)penta-1,4-dien-3-one (**11a**).* Yellow solid, yield 76.4%; mp: ºC; IR (KBr, cm^{-1}): 3149.1, 3049.9, 2988.4, 1644.7, 1610.7, 1338.5, 961.9; ^1H NMR (500 MHz, $CDCl_3$+ DMSO-d_6): δ 8.58 (s, 1H), 8.11–8.00 (m, 1H), 7.75–7.28 (m, 10H), 7.19–7.01 (m, 2H); ^{13}C NMR (125 MHz, $CDCl_3$+ DMSO-d_6): δ 188.2, 139.8, 138.5, 137.9, 135.3, 134.0, 132.4, 129.8, 129.1, 126.9, 125.4, 122.9, 121.3, 120.6, 120.4, 113.1, 112.7; HRMS (ESI): *m/z* calcd for $C_{19}H_{15}ClNO$ 308.0837, found 308.0835 $[M+H]^+$.

*4.2.8.21. (1E,4E)-1-(1H-indol-3-yl)-5-(4-methoxyphenyl)penta-1,4-dien-3-one (**11b**).* Yellow solid, yield 72.1%; mp: 163–165 °C; IR (KBr, cm^{-1}): 3123.5, 2987.9, 2929.7, 1647.5, 1585.8, 1332.3, 1100.6, 983.2; ^1H NMR (500 MHz, $CDCl_3$+DMSO-d_6): δ 10.37 (s, 1H), 8.14–7.30 (m, 7H), 7.25–6.68 (m, 6H), 3.83 (s, 3H); ^{13}C NMR (125 MHz, $CDCl_3$+ DMSO-d_6): δ 189.0, 161.2, 141.5, 137.7, 137.5, 130.9, 129.9, 127.8, 125.4, 124.0, 122.9, 121.2, 121.0, 120.4, 114.3, 113.6, 112.3, 55.3; HRMS (ESI): *m/z* calcd for $C_{20}H_{18}NO_2$ 304.1332, found 304.1327 $[M+H]^+$.

*4.2.8.22. (1E,4E)-1-(2,5-dimethoxyphenyl)-5-(1H-indol-3-yl)penta-1,4-dien-3-one (**11c**).* Yellow solid, yield 70%; mp: 98–100 °C; IR (KBr, cm^{-1}): 3123.7, 2987.9, 2930.1, 1647.5, 1585.7, 1332.3, 1100.4, 983.1; ^1H NMR (500 MHz, $CDCl_3$+ DMSO-d_6): δ 10.05 (s, 1H), 8.06–7.96 (m, 2H), 7.61–7.57 (m, 1H), 7.35–7.28 (m, 3H), 7.21–6.82 (m, 6H), 3.87 (s, 3H), 3.82 (s, 3H); ^{13}C NMR (125 MHz, $CDCl_3$+ DMSO-d_6): δ 189.8, 153.5, 153.1, 137.5, 137.4, 130.2, 127.0, 124.3, 123.4, 122.9, 121.4, 121.6, 120.6, 117.1, 114.2, 113.0, 112.5, 56.1, 55.8; HRMS (ESI): *m/z* calcd for $C_{21}H_{20}NO_3$ 334.1438, found 334.1442 $[M+H]^+$.

*4.2.8.23. (1E,4E)-1-(3,4-dimethoxyphenyl)-5-(1H-indol-3-yl)penta-1,4-dien-3-one (**11d**).* Yellow solid, yield 72.3%; mp: 136–138 °C; IR (KBr, cm^{-1}): 3179.2, 3111.2, 2970.2, 1634.9, 1610.8, 1358.9, 1262.1, 982.0; ^1H NMR (500 MHz, $CDCl_3$+ DMSO-d_6): δ 10.70 (s, 1H), 8.04–7.85 (m, 2H), 7.68–7.30 (m, 3H), 7.25–6.73 (m, 7H), 3.88 (s, 3H), 3.85 (s, 3H); ^{13}C NMR (125 MHz, $CDCl_3$+ DMSO-d_6): δ 188.7, 150.9, 149.1, 141.7, 137.7, 131.2, 128.0, 125.3, 124.3, 122.8, 121.1, 120.6, 120.3, 113.4, 112.3, 111.1, 109.7, 55.9; HRMS (ESI): *m/z* calcd for $C_{21}H_{20}NO_3$ 334.1438, found 334.1435 $[M+H]^+$.

*4.2.8.24. (1E,4E)-1-(1H-indol-3-yl)-5-(2,4,6-trimethoxyphenyl) penta-1,4-dien-3-one (**11e**).* Yellow solid, yield 74.1%; mp: 226–228 °C; IR (KBr, cm^{-1}): 3123.7, 2987.9, 2929.9, 1647.5, 1585.5, 1332.2, 1100.3, 983.1; ^1H NMR (500 MHz, $CDCl_3$+DMSO-d_6): δ 8.51 (s, 1H), 8.20 (d, *J* = 16.1 Hz, 1H), 8.06–7.94 (m, 2H), 7.61–7.27 (m, 5H), 7.18 (d, *J* = 15.8 Hz, 1H), 6.15 (s, 2H), 3.96–3.82 (m, 9H); ^{13}C NMR (125 MHz, $CDCl_3$+DMSO-d_6): δ 189.6, 162.1, 160.6, 136.9, 132.3, 130.0, 125.5, 124.7, 121.9, 120.8, 120.2, 119.5, 112.6, 111.6, 105.4, 89.8, 55.1, 54.6; HRMS (ESI): *m/z* calcd for $C_{22}H_{22}NO_4$ 364.1543, found 364.1539 $[M+H]^+$.

*4.2.8.25. (1E,4E)-1-(1H-indol-3-yl)-5-(3,4,5-trimethoxyphenyl) penta-1,4-dien-3-one (**11f**).* Yellow solid, yield 70.2%; mp: 166–168 °C; IR (KBr, cm^{-1}): 3240.1, 2988.5, 2901.7, 1638.8, 1608.6, 1332.6, 1100.4, 981.1; ^1H NMR (500 MHz, $CDCl_3$+DMSO-d_6): δ 11.47 (s, 1H), 8.11–7.92 (m, 2H), 7.77–7.66 (m, 3H), 7.63 (d, *J* = 15.7 Hz, 1H), 7.48 (s, 1H), 7.25 (s, 1H), 7.10 (d, *J* = 15.7 Hz, 2H), 6.94 (s, 1H), 3.93 (s, 6H), 3.85 (s, 3H); ^{13}C NMR (125 MHz, $CDCl_3$+ DMSO-d_6): δ 187.1, 152.1, 140.3, 138.5, 136.7, 130.7, 129.5, 124.6, 124.1, 121.6, 120.0, 119.2, 111.9, 111.3, 104.3, 59.4, 54.9; HRMS (ESI): *m/z* calcd for $C_{22}H_{22}NO_4$ 364.1543, found 364.1547 $[M+H]^+$.

4.3. Biological evaluation

4.3.1. Cell cultures

The lung (A549), breast (MDA-MB-231, BT549 and 4T1), prostate (PC-3, DU145), gastric (HGC-27) and cervical (HeLa) tumor cell lines were obtained from National center for Cell science (NCCS), Pune, India. MTT [3-(4, 5-dimethylthiazol-2-yl)-2, 5-diphenyl tetrazolium bromide], Trypsin-EDTA were purchased from Sigma Chemicals Co (St. Louis, MO). DMEM, RPMI 1640 medium, Fetal bovine serum were purchased from GIBCO-Invitrogen. The 12, 24 and 96 well flat bottom tissue culture plates were purchased from Corning.

4.3.2. MTT assay

The cytotoxic activity of the compounds (**9a-s**, **11a-f**) was determined by using MTT assay. 5×10^3 cells per well were seeded in 100 μL DMEM or RPMI, supplemented with 10% FBS in each well of 96-well microculture plates and incubated for 24 h at 37 °C in a CO_2 incubator. Compounds, diluted to the desired concentrations in culture medium, were added to the wells with respective vehicle control. After 48 h of incubation, medium was removed, 100 μL of MTT (3-(4,5-dimethylthiazol-2-yl)- 2,5-diphenyl tetrazolium bromide) (0.5 mg mL^{-1}) containing medium was added to each well and the plates were further incubated for 4 h. Then, the supernatant from each well was carefully removed, formazon crystals were dissolved in 200 μL of DMSO and absorbance was recorded at 570 nm wavelength with multimode plate reader (Spectramax M4, Molecular devices, USA).

4.3.3. Evaluation of tubulin polymerization inhibitory activity

Tubulin polymerization kit was purchased from Cytoskeleton, Inc. (BK011). To evaluate the effect of compound **11c**, **11d** and **11f** on tubulin assembly, a fluorescence based *in vitro* tubulin polymerization assay was conducted following the manufacturer's protocol. The reaction mixture having porcine brain tissue (2 mg/mL) in 80 mM PIPES at pH 6.9, 2.0 mM $MgCl_2$, 0.5 mM EGTA,1.0 mM GTP and glycerol in the presence and absence of test compounds (final concentration of 10 μM) was prepared and added to each well of 96-well plate. Tubulin polymerization was followed by a time dependent increase in fluorescence due to the incorporation of a fluorescence reporter into microtubules as polymerization proceeds. Fluorescence emission at 440 nm (excitation wavelength is 360 nm) was measured by using a Spectramax M4 Multi mode Micro plate Detection System. Nocodazole was used as positive control in the assay. The IC50 value was calculated from the drug concentration required for inhibiting 50% of tubulin assembly compared to control.

4.3.3.1. Acridine orange/ethidium bromide (AO/EB) staining. The morphological changes of treated and control cells were examined by Acridine Orange/Ethidium Bromide (AO/EB) staining. PC-3 cells were grown in 24 well plates (25,000 cells/well) for 24 h

and were treated with 2.5 and 5 μM concentration of compound **11c** and **11f** for 48 h. After the incubation, medium was removed, washed with PBS and treated with dyes 10 μg/ml acridine orange and 10 μg/mL ethidium bromide. Morphological features were observed and photographs were taken immediately under fluorescence inverted microscope (Model: Nikon, Japan) with excitation (488 nm) and emission (550 nm) at 200× maginification.

4.3.3.2. DAPI staining. Human prostate cancer PC-3 cells were seeded on 24 well plates at the density of 25,000 cells/well and allowed to adhere overnight. Then cells were treated with 2.5 and 5 μM concentration of compound **11c** and **11f** for 48 h, washed with PBS and fixed with 4% neutral buffered formalin solution for 20 min. Then, cells were washed twice with PBS and permeabilized with 0.2% triton-x for 5min and stained with DAPI (1 μg/mL) for 10 min at room temperature. Cells were examined for morphological changes under fluorescence microscope (Model: Nikon, Japan) using 350 nm excitation and 460 nm emission at 200× magnification.

4.3.3.3. Measurement of mitochondrial membrane potential (MMP). PC-3 cells were cultured in 12 well plates at a density of 1×10^5 cells/mL and allowed to grow overnight. The cells were treated with 5 μM of compounds **11c** and **11f**. After 24 h of incubation, cells were treated with PBS containing JC-1 (2 μM) dye for 45 min in dark at 37° C in incubator. Subsequently, dye was removed by washing with PBS twice and the samples were analyzed for fluorescence using spectroflourometer. Fluorescence was assessed at excitation wavelength (540 nm) and emission wavelength (590 nm) with the Multimode Plate Reader (Spectramax M4, Molecular devices, USA). The change in mitochondrial membrane potential is represented by the ratio of fluorescence readings at 540 (green) and at 590 nm (red).

4.3.4. Flow-cytometry analysis

To determine the effect of compounds **11c** and **11f** on the cell cycle, cells were seeded in 12-well plates at a density of 1×10^5 cells/mL and allowed to attach for 24 h. After incubation, cells were treated with desired concentrations of compounds **11c** and **11f** and incubated for 24 h. Then the cells were collected, washed and fixed in 70% ethanol in PBS at −20 °C. After leaving overnight, the fixed cells were pelleted and stained with Propidium Iodide (25 μg/ml)) in the presence of RNase A (40 μg/mL) containing 0.1% Triton X-100 for 30 min at 37 °C in dark, and about 10,000 events were analyzed on a flow cytometry (FACS verse, Becton Dickinson, US).

4.4. Molecular modelling studies

The crystal co-ordinates of α,β-tubulin subunits were retrieved from the protein data bank (PDB ID: 3E22) [48]. As the active site i.e., colchicine binding site of tubulin is located at the interface of α,β-tubulin subunits, both the α,β chains were considered for molecular modelling studies [49]. The Schrödinger's (Schrödinger L.L.C., USA) protein preparation tool i.e., protein preparation tool was used for the preparation of receptor model. The tool adds missing side chains and loops and also removes water molecules with a distance of more than 5 Å. Then, restrained minimization was performed utilizing the OPLS 2005 force field to RMSD of 0.3 Å and an active site pocket of colchicine with 20 Å equally in each direction of X, Y, and Z was used for receptor grid generation. The potential ligands **11c** and **11f** were sketched by using 2D sketcher and, prepared for docking using Ligprep and a total number of 10 conformers were generated for each of the ligand. The ligands **11c** and **11f** were docked into the active site of tubulin using GLIDE-XP (Extra Precision) flexible program. The best model was picked based on the best stabilization energy as shown in Fig. 12.

Acknowledgements

P.V.S. and A.S. are thankful to DoP, Ministry of Chemicals & Fertilizers, Govt. of India, New Delhi, for the award of NIPER fellowship.

Appendix A. Supplementary data

Supplementary data related to this article can be found at http://dx.doi.org/10.1016/j.ejmech.2016.12.043.

References

[1] H. Hatcher, R. Planalp, J. Cho, F.M. Torti, S.V. Torti, Cell. Mol. Life Sci. 65 (2008) 1631–1652.
[2] S. Luer, R. Troller, C. Aebi, Nutr. Cancer 64 (2012) 975–981.
[3] C.H. Liu, H.Y. Huang, Chem. Pharm. Bull. 60 (2012) 1118–1124.
[4] B.B. Aggarwal, A. Kumar, A.C. Bharti, Anticancer Res. 23 (2003) 363–398.
[5] T. Masuda, T. Maekawa, K. Hidaka, H. Bando, Y. Takeda, H. Yamaguchi, J. Agric. Food Chem. 49 (2001) 2539–2547.
[6] N. Chainani-Wu, J. Altern, Complement. Med. 9 (2009) 161–168.
[7] P. Basnet, N. Skalko-Basnet, Molecules 16 (2011) 4567–4598.
[8] W.C. Jordan, C.R. Drew, J. Natl, Med. Assoc. 88 (1996) 333.
[9] E. Cretu, A. Trifan, A. Vasincu, A. Miron, Rev. Med. Chir. Soc. Med. Nat. Iasi 116 (2012) 1223–1229.
[10] L. Lin, Q. Shi, C.Y. Su, C.C. Shih, K.H. Lee, Bioorg. Med. Chem. 14 (2006) 2527–2534.
[11] B.B. Aggarwal, Cancer Biol. Ther. 7 (2008) 1436–1440.
[12] D. Nambiar, R.P. Singh, Nutr. Cancer 65 (2013) 12–25.
[13] R.A. Sharma, H.R. McLelland, K.A. Hill, C.R. Ireson, S.A. Euden, M.M. Manson, M. Pirmohamed, L.J. Marnett, A.J. Gescher, W.P. Steward, Clin. Cancer Res. 7 (2001) 1894–1900.
[14] D.K. Agrawal, P.K. Mishra, Med. Res. Rev. 30 (2010) 818–860.
[15] M. Mimeault, S.K. Batra, Chin. Med. 6 (2011) 31.
[16] J.R. Dimmock, M.P. Padmanilayam, R.N. Puthucode, A.J. Nazarali, N.L. Motaganahalli, G.A. Zello, J.W. Quail, E.O. Oloo, H.B. Kraatz, J.S. Prisciak, T.M. Allen, C.L. Santos, J. Balzarini, E. De Clercq, E.K. Manavathu, J. Med. Chem. 44 (2001) 586–593.
[17] L. Lin, B. Hutzen, S. Ball, E. Foust, M. Sobo, S. Deangelis, B. Pandit, L. Friedman, C. Li, P.K. Li, J. Fuchs, J. Lin, Cancer Sci. 100 (2009) 1719–1727.
[18] N. Samaan, Q. Zhong, J. Fernandez, G. Chen, A.M. Hussain, S. Zheng, G. Wang, Q.-H. Chen, Eur. J. Med. Chem. 75 (2014) 123–131.
[19] H. Luo, S. Yang, Y. Cai, Z. Peng, T. Liu, Eur. J. Med. Chem. 84 (2014) 746–752.
[20] B.-F. Ruan, X. Lu, T.-T. Li, J.-F. Tang, Y. Wei, X.-L. Wang, S.-L. Zheng, R.-S. Yao, H.-L. Zhu, Bioorg. Med. Chem. 20 (2012) 1113–1121.
[21] N.K. Paul, M. Jha, K.S. Bhullar, H.P.V. Rupasinghe, J. Balzarini, A. Jha, Eur. J. Med. Chem. 87 (2014) 461–470.
[22] R. Wang, C. Chen, X. Zhang, C. Zhang, Q. Zhong, G. Chen, Q. Zhang, S. Zheng, G. Wang, Q.-H. Chen, J. Med. Chem. 58 (2015) 4713–4726.
[23] Q.-H. Chen, K. Yu, X. Zhang, G. Chen, A. Hoover, F. Leon, R. Wang, N. Subrahmanyam, E.A. Mekuria, L.H. Rakotondraibe, Bioorg. Med. Chem. Lett. 25 (2015) 4553–4556.
[24] P. Rani, V.K. Srivastava, A. Kumar, Eur. J. Med. Chem. 39 (2004) 449–452.
[25] Y.M.A. Hiari, A.M. Qaisi, M.M. Abadelah, W. Voelter, Monatsh. Fur Chem. 137 (2006) 243–248.
[26] L.C. Garcia, R. Martinez, Eur. J. Med. Chem. 37 (2002) 261–266.
[27] I. Merino, A. Monge, M. Font, J.J.M. Irujo, E. Alberdi, E. Santiago, I. Prieto, J. Lasarte, P. Sarobe, F. Borras, Il Farm. 54 (1999) 255–264.
[28] O. Talaz, I. Gulcin, S. Goksu, N. Saracoglu, Bioorg. Med. Chem. 217 (2009) 6583–6589.
[29] N. Karali, A. Gursoy, F. Kandemirli, N. Shvets, F.B. Kaynak, S. Ozbey, V. Kovalishyn, A. Dimoglo, Bioorg. Med. Chem. 15 (2007) 5888–5904.
[30] J. Hooker, W. Bogdanich, New York Times, 2008.
[31] M.A. Jordan, W. Leslie, Nat. Rev. Cancer 1 (2004).
[32] H.M. Prince, M. Bishton, Hematology Meeting Reports, vol. 3, 2009, pp. 33–38.
[33] P. Cook, I. James, N. Engl, J. Med. 305 (1981) 1560–1564.
[34] M.T. Isaac, Evid. Based Ment. Health 7 (2004) 107.
[35] G.D. Morse, R.C. Reichman, M.A. Fischl, Antivir. Res. 45 (2000) 47–58.
[36] A.G. Romero, J.A. Leiby, R.B. McCall, M.F. Piercey, M.W. Smith, F. Han, J. Med, Chem. 36 (1993) 2066–2074.
[37] D.E. Ward, C.K. Rhee, Can. J. Chem. 67 (1989) 1206–1211.
[38] M. Senoo, A. Furukawa, T. Hata, H. Urabe, Chem. - A Eur. J. 22 (2015) 890–895.
[39] M. Amel, A.-B. Abdelhakim, Y. Wei, H. Romain, C. Marie, B. Rozenn, P. Jean-Michel, B. Ahcene, P. Marine, Eur. J. Med. Chem. 80 (2014) 579–592.
[40] Q. Nan, L. Chun-Bao, J. Mei-Na, S. Li-Huan, D. Hong-Quan, N. Wen-Yan, Eur. J. Med. Chem. 46 (2011) 5189–5195.
[41] V. Naidu, U.M. Bandari, A.K. Giddam, K.R.D. Babu, J. Ding, K.S. Babu, B. Ramesh,

R.R. Pragada, P. Gopalakrishnakone, Asian Pac. J. Trop. Med. (2013) 337–345.
[42] H. Mirzaei, S. Emami, Eur. J. Med. Chem. 121 (2016) 610–639.
[43] Z. Wang, H. Qi, Q. Shen, G. Lu, M. Li, K. Bao, Y. Wu, W. Zhang, Eur. J. Med. Chem. 122 (2016) 520–529.
[44] B. Sun, L. Li, Q.-W. Hu, F. Xie, H.-B. Zheng, H.-M. Niu, H.-Q. Yuan, H.-X. Lou, Eur. J. Med. Chem. 121 (2016) 484–499.
[45] D. Ribble, N.B. Goldstein, D.A. Norris, Y.G. Shellman, BMC Biotechnol. (2005) 5.
[46] Y.H. Wong, A.K. Habash, Evidence-Based Complementary Altern. Med. (2011) 13, http://dx.doi.org/10.1155/2011/293060. Article ID 293060.
[47] U.V. Mallavadhani, C.V. Prasad, S. Shrivastava, V. Naidu, Eur. J. Med. Chem. 83 (2014) 84–91.
[48] A. Kamal, A.B. Shaik, N. Jain, C. Kishor, A. Nagabhushana, B. Supriya, G.B. Kumar, S.S. Chourasiya, Y. Suresh, R.K. Mishra, A. Addlagatta, Eur. J. Med. Chem. 92 (2015) 501–513.
[49] R.B. Ravelli, B. Gigant, P.A. Curmi, I. Jourdain, S. Lachkar, A. Sobel, M. Knossow, Nature 428 (2004) 198–202.